論文 / 著書情報
Article / Book Information

題目(和文)	
Title(English)	Tumoral Acidic pH-responsive Polycarboxybetaine-coated Lipid Nanoparticle for Effective siRNA Delivery
著者(和文)	SUNGYi-Jung
Author(English)	Yijung Sung
出典(和文)	学位:博士(学術), 学位授与機関:東京工業大学, 報告番号:甲第12301号, 授与年月日:2022年12月31日, 学位の種別:課程博士, 審査員:西山 伸宏,三浦 裕,小畠 英理,曽根 正人,栁田 保子,小倉 俊一郎
Citation(English)	Degree:Doctor (Academic), Conferring organization: Tokyo Institute of Technology, Report number:甲第12301号, Conferred date:2022/12/31, Degree Type:Course doctor, Examiner:,,,,,
学位種別(和文)	博士論文
Type(English)	Doctoral Thesis

Tumoral Acidic pH-responsive Polycarboxybetaine-coated Lipid Nanoparticle for Effective siRNA Delivery

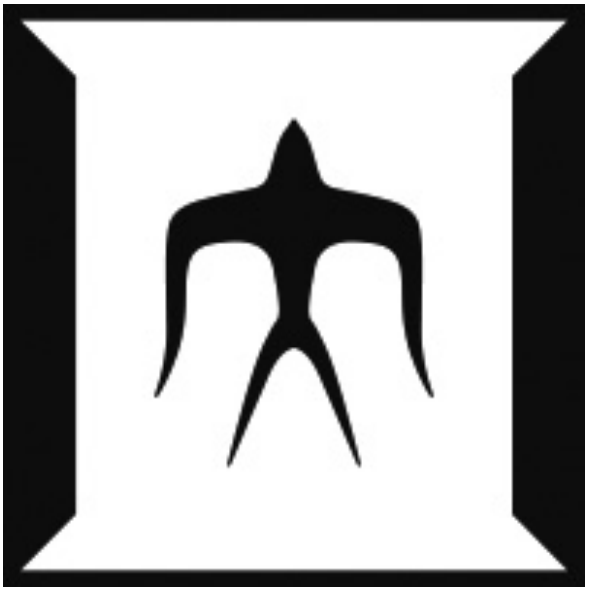

Doctoral Thesis

Yi-Jung Sung

Aceramic Supervisor: Dr. Nobuhiro Nishiyama

Department of Life Science and Technology
School of Life Science and Technology
Tokyo Institute of Technology

2022

Abstract

Lipid nanoparticles (LNPs) have been commonly used as a vehicle of nucleic acids such as small interfering RNA (siRNA), and the surface modification of LNPs is one of the determinants on their delivery efficiency especially in the systemic administration. Poly(ethylene glycol) (PEG) modification of pharmaceutics, namely PEGylation, is the most common strategy to prolong circulation time. However, PEG shell potentially hinders the interaction with target cells and endosomal membrane. Lacking target ability, LNP would be difficult to deliver to target site. Here, we report a smart surface modification employing a charge-switchable ethylenediamine-based polycarboxybetaine for enhancing tumor accumulation *via* interaction with anionic tumorous tissue-constituents owing to selective switch to cationic charge in response to cancerous acidic pH. This polycarboxybetaine-modified LNP could enhance cellular uptake in cancerous pH, resulting in facilitated endosomal escape and gene knockdown efficiency. After systemic administration, the polycarboxybetaine-modified LNP accomplished higher tumor accumulation than positive control LNP in subcutaneous tumor models. The siPLK-1-encapsulated LNP thereby accomplished significant tumor growth

inhibition. This study demonstrates a promising potential of the pH-responsive polycarboxybetaine as the material modifying the surface of LNPs for efficient nucleic acid delivery.

Keywords:

Lipid nanoparticle; pH-Responsiveness; Polycarboxybetaine; siRNA

Acknowledgement

The complement of this thesis thanks to the support of many individuals.

First and foremost, I truly appreciate that Professor Nobuhiro Nishiyama allowed me to challenge such innovative research; therefore, I am honored to become the pioneer of building nucleic acid/lipid nanoparticle system in this laboratory. Moreover, I have been getting insightful advice and ideas when discussing with Prof. Nishiyama throughout my research. I am also thankful for his supports not only in research but also in every aspect from scholarship application to consultation of entrance examination.

Next, I want to express my gratitude to my mentors Dr. Hiroyasu Takemoto and Dr. Yutaka Miura. This study would not be completed without there assistance. I learned from Dr. Takemoto how important it is to predict success or failure based on knowledge and experiences before starting any experiment. His honest feelings towards students let our group start to gel. Dr. Miura's research enthusiasm always inspires me. I deeply realized that knowledge and ability are everything regardless of the position. Importantly, I really learned a crucial lesson from Dr. Miura about the importance of dispersing responsibility as well as sharing achievements. I will remember their grace forever.

In addition, I would not forget to thank Dr. Takahiro Nomoto, Dr. Makoto Matusi, Mr. Haochen Guo, Ms. Xin Shen and Mr. Kaito Kanamori for their helpful suggestion. Especially, the advice given from Dr. Nomoto played an important role in this research. That is why I respect him very much. I can't thank Mr. Guo and Ms. Xin Shen enough because this research was impossible to proceed so smoothly without discussion with them. When I was upset in the dark moment, Haochen and Dr. Nomoto's kindness and wisdom always provided me with motivation to move forward.

Last but not least, I would like to thank all my friends in Nishiyama laboratory for their emotional supports especially to Aria, Ping, Motoaki, Takumi, Andrew, Voon, Zhou, Ema, Miyazaki, Tokura, Dewa, Komoto, Alvin and Iwata. They are always rooting for me and push me through the stressful times. My friends and families outside of this lab are also worthy of my sincerest appreciation.

Table of Content

Table of Figures

Table of tables

Abbreviation

Abbreviation	Full name
AcN	Acetonitrile
ApoE	Apolipoprotein E
CLSM	Confocal laser scanning microscope
CT26	Murine colorectal carcinoma cell line
D_2O	Deuterium oxide
DBCO	Dibenzocyclooctyl
DCM	Dichloromethane
DCl	Deuterium chloride
DLS	Dynamic laser scanning
DMEM	Dulbecco's Modified Eagle Medium
DOPC	1,2-dioleoyl-sn-glycero-3-phosphocholine
DOPE	1,2-dioleoyl-sn-glycero-3-phosphoethanolamine
DODAP	1,2-dioleoyl-3-dimethyaminopropane
DOTAP	1,2-dioleoyl-3-trimethylammonium-propane
DSPC	distearoylphosphatidylcholine

DSPE	1,2-Distearoyl-sn-glycero-3-phosphorylethanolamine
dsRNA	Double-strand RNA
EE	Encapsulation efficiency
EPR	Enhanced permeation and retention
FBS	Fetal bovine serum
FCM	Flow cytometer
FI	Fluorescence intensity
HCl	Hydrochloric acid
HEPES	4-(2-hydroxyethyl)-1-piperazineethanesulfonic acid
HPLC	High performance liquid chromatography
i.p	Intraperitoneal
i.v	Intravenous
IVIS	*In vivo* imaging system
LNP	Lipid nanoparticle
MC3	DLin-MC3-DMA
MES	2-(*N*-morpholino)ethanesulfonic acid
MPS	mononuclear phagocyte system
mRNA	Messenger RNA
NT	Non-treatment

PBS	Phosphate buffered saline
PCR	Polymerase chain reaction
PDI	Polydispersity
PEG	Poly(ethylene glycol)
PE	Phosphorylethanolamine
RES	Reticuloendothelial system
RISC	RNA-Induced Silencing Complex
RNAi	RNA interference
RT	Reverse transcription
RT-PCR	Reverse transcription polymerase chain reaction
r.t.	Room temperature
RUL	Relative luminescence units
SD	Standard deviation
SEM	Standard error of mean
SKOV3-luc	Luciferase expression human ovary cancer cell line SKOV-3
siRNA	short interfering RNA
t-BuOH	tert-butanol
TEM	Transmission electron microscopy

THF	tetrahydrofuran

Chapter 1 Introduction

1.1 Small interference RNA delivery in cancer therapy

1.1.1 RNA interference (RNAi) and small interference RNA (siRNA)

RNA interference mechanism was discovered in 1998 by Andrew Fire [1]. Andrew Fire and Craig C. Mello won the 2006 Nobel Prize for their great contribution to RNAi [1]. Transcriptional gene silencing was reported by Andrew Hamilton and David Baulcombe and in 1999 [2]. In 2001, Thomas Tuschl's group successfully induced RNAi in mammalian cells with synthetic siRNAs [3]. siRNA is a double-stranded RNA (dsRNA) having the function of RNAi which suppress the expression of specific gene. The mechanism of gene silencing *via* suppression of translation is shown in Fig. 1.1. When dsRNA entered cytoplasm, Dicer which is an endoribonuclease would cut dsRNA to short interfering RNA (siRNA) [4]. Proteins such as ribonucleoprotein incorporate with siRNA to form RNA-Induced Silencing Complex (RISC) [5], and then siRNA is unwound to form single stranded siRNA which can recognize the complementary messenger (mRNA). mRNA cleavage was induced when single stranded siRNA binds to the target mRNA.

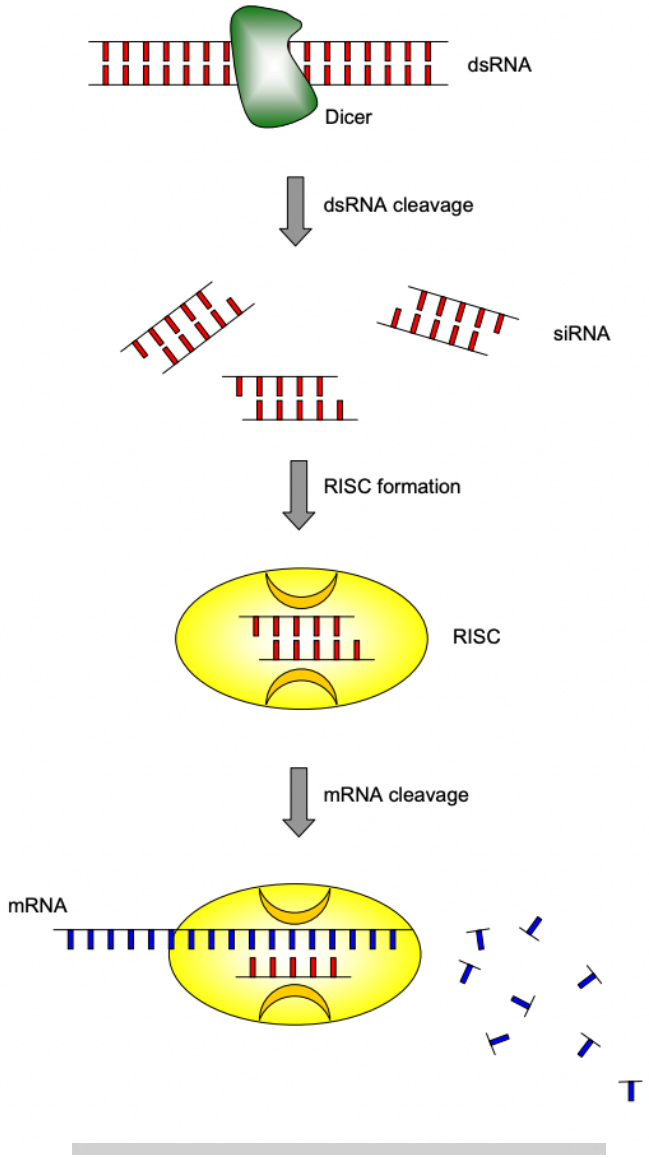

Figure 1.1 Mechanism of RNAi [6].

Gene silencing results from no translation of mRNA into amino acids and proteins due to the degradation of mRNA [6]. Therefore, siRNA can knockdown certain protein expression and is potential to highly expressed protein in cancer cell.

1.1.2 siRNA delivery and Lipid-based carrier

siRNA became a potential treatment since tremendous progress in RNAi development. However, siRNA medicine has critical challenges including rapid degradation by RNases, quick clearance and poor cell penetration [7, 8] which cover up the powerful light of gene silencing. Besides the numerous *in vivo* barriers like clearance from immune system, the highly negative charge of siRNA generates the repulsion from similarly charged cell membrane as well as plasma membrane. Therefore, better carriers to protect siRNA and deliver to target site is a *sine qua non* for siRNA delivery.

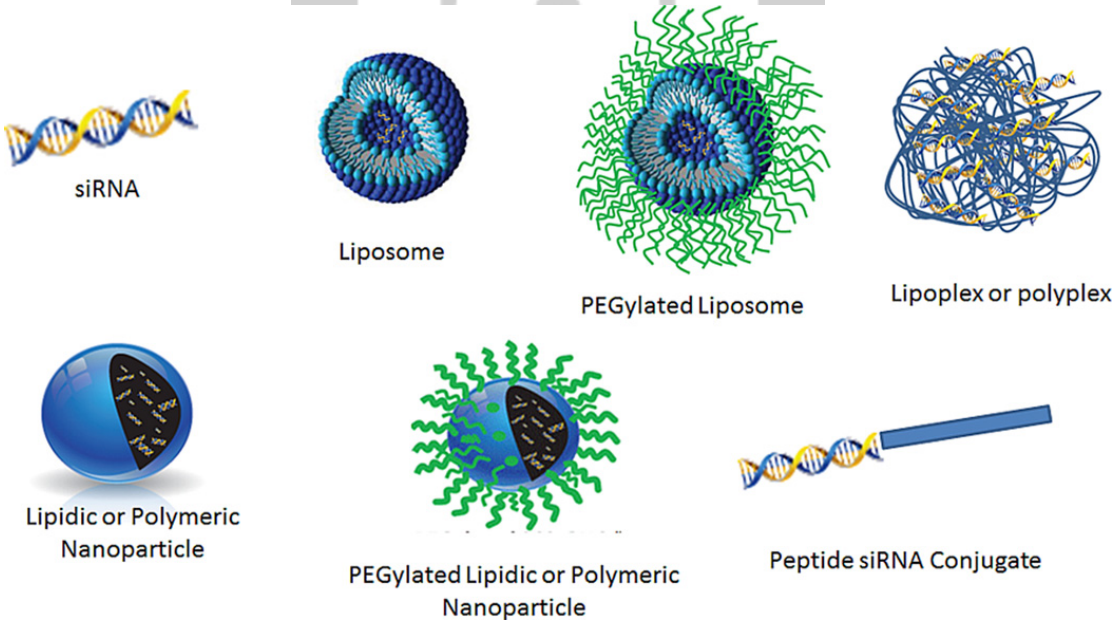

Figure 1.2 Schematic of different non-viral siRNA delivery vectors [9].

In recent years, nanocarriers have been widely used for siRNA delivery

(Fig. 1.2) such as virus vector, polymer complex and lipid nanoparticle (LNP) [9, 10]. The advantages of nanoparticles in siRNA delivery are, for example, increasing stability, prolonged half-life in blood circulation and preferential tumor targeting by an Enhanced Permeation and Retention (EPR) effect especially for cancer therapy [11]. Among these nanocarriers, lipid-based nanoparticles were highlight as a lead system for siRNA delivery due to its low toxicity [12]. Lipid-based nanoparticle systems have evolved substantially over the past two decades thanks to the biodegradable nature and low toxicity of the lipid materials [13]. In 2018, FDA approved the first-ever siRNA medicine, Patisiran (Onpattro®), for the treatment of polyneuropathy with hereditary transthyretin-mediated amyloidosis, which represents a milestone in siRNA therapeutics [14, 15]. Patisitan has ignited optimism about lipid-based nanoparticle as a potential siRNA delivery payload owing to its cleavable PEG-lipid PEG-DMG and newly ionizable lipid DLin-MC3-DMA (MC3). Cleavable PEG-DMG protected LNP during circulation [14, 15] and improved uptake through PEG cleavage [14, 15] to avoid PEG dilemma as described in chapter 1.2. When PEG dropped off, hydrophobic lipid shell could be adsorbed by Apolipoprotein E (ApoE) which is ligand for ApoE receptor in hepatocyte. MC3 had pKa 6.44 [16] to facilitate endosomal escape which will be further discuss in chapter 1.4.

Although siRNA has been considered one of the most noteworthy treatments which can regulate gene expression, the applications are limited due to lacking effective systems to deliver to target tissues other than liver. Researchers still have been trying to accomplish siRNA treatment in cancer therapy.

1.2 Tumor targeting

1.2.1 Blood clearance

The main limitation of siRNA-encapsulated LNP delivery is inability to reach tumor sites due to nonspecific nanoparticle uptake by organs. The mononuclear phagocyte system (MPS) also known as the reticuloendothelial system (RES) consists of the phagocytic cells which accumulate in liver, spleen and lymph nodes [17, 18]. After administration of LNP, it would be immediately sequestered by MPS, which involves adsorption of plasma protein affected by particle size, hydrophobicity and surface chemistry [19, 20]. For instance, large nanocarrier (> 200 nm) was reported to highly accumulate in spleen and liver [18], and small particles (< 5 nm) would be quickly undergo renal clearance [21]. Highly cationic nanoparticles are rapidly cleared from blood circulation compared to slight negative and neutral particles [18, 22] despite the benefit of

positive charge to facilitated cellular uptake.

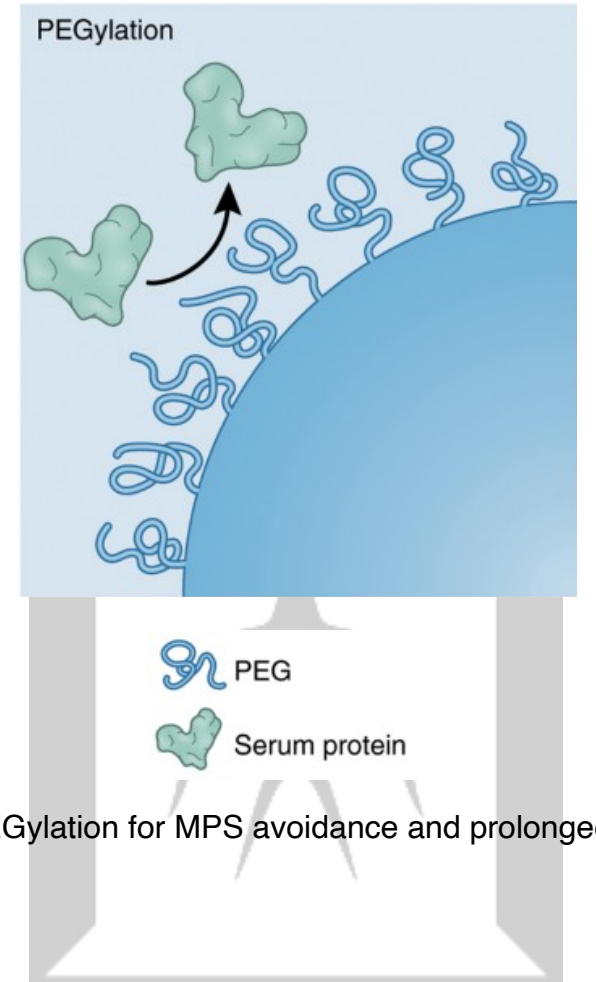

Figure 1.3 PEGylation for MPS avoidance and prolonged circulation [18].

In addition to controlling characterizations of particle, one common strategy is grafting poly(ethylene glycol) (PEG) onto nanoparticle surface, also called PEGylation (Fig. 1.3), where ethylene glycol units form hydrating layer with water molecules which hinders protein adsorption and prevent clearance by MPS [23]. However, high density of PEG might lead to inefficient cellular uptake, which is called PEG dilemma [24, 25].

1.2.2 Passive targeting and EPR effect

Nanoparticles can transport to tumor through leaky vessels by diffusion or convection as Fig. 1.4 showed, which termed “passive” mainly relies on tumor biology and characteristics of particle [26, 27]. Enhanced Permeation and Retention (EPR) effect, first discovered by Maeda in 1986 [28], has played an important role in retaining the therapeutic agent in cancer. In normal tissue, the junctions of endothelial cells are tight, and therapeutics are not allowed to transport across them as Fig. 1.5 showed. In contrast, aberrant vascular architecture creates a loose and leaky junction (Fig. 1.5) due to lacking lymphatic drainage and overproduction of vascular permeability factors which stimulates the extravasation within tumor tissue. The special phenomenon provides an opportunity for macromolecules like nanoparticles to accumulate in tumors [18, 26, 27, 29].

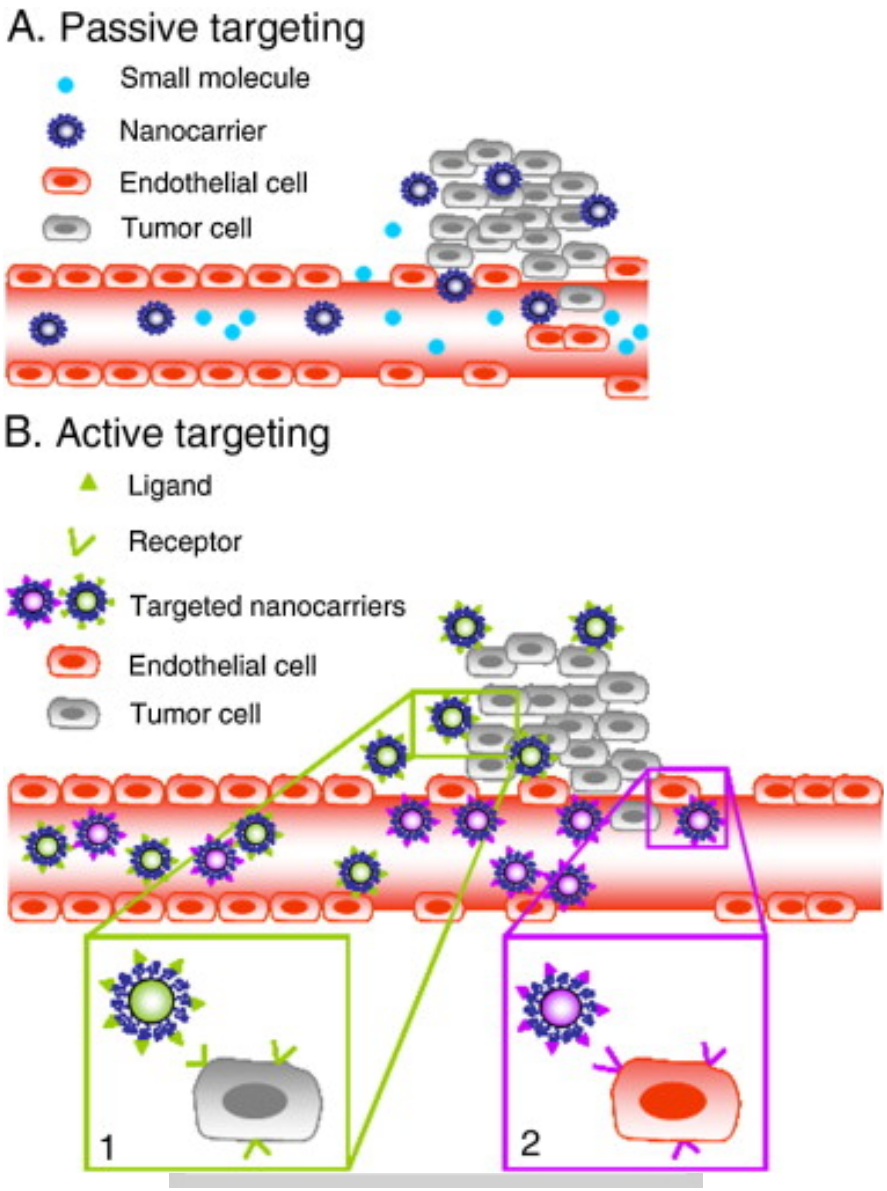

Figure 1.4 Illustration of tumor passive and active targeting [27]

Generally, 10 to 100 nm particles were found efficient accumulation in animal model *via* passive target [29]. Indeed, transporting siRNA *via* EPR effect is sometimes not very effective due to the heterogeneity and EPR effect level among tumors which might be influenced by interstitial fluid pressure, vessel density and tumor type [30-34].

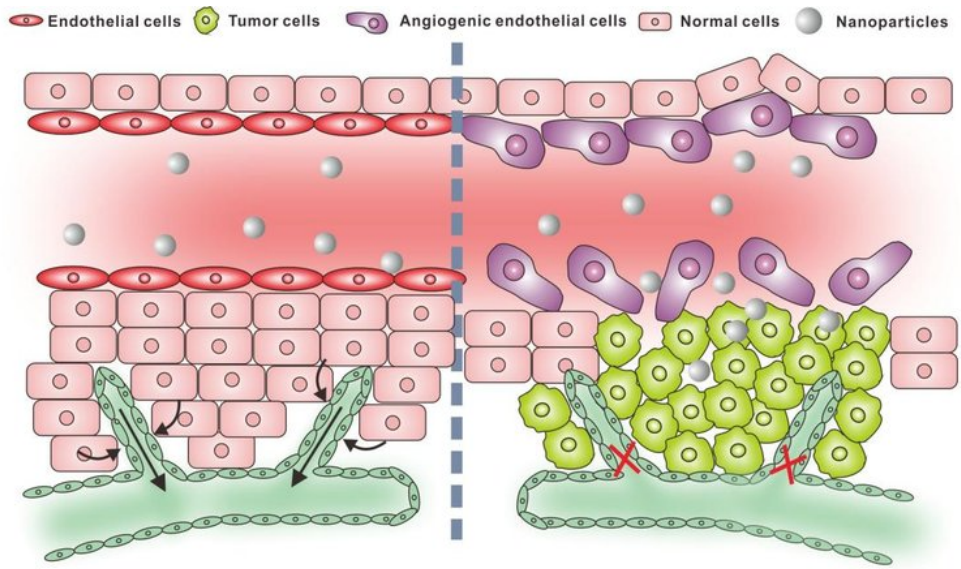

Figure 1.5 Different endothelial cell junction between normal tissue and tumor tissue [35]

Thus, the ability for pinpoint tumor targeting together with efficient nucleic acid transfection is essential for a successful LNP system.

1.3 Tumor microenvironment

1.3.1 Tumor acidic pH

Tumor targeting can be improved through employing tumor-specific conditions. Extracellular acidic pH of tumor microenvironment is a prevalent characteristic which results from hypoxia as well as rapid glycolysis and lactate production [36-40]. In proliferating cells such as tumor cells, the glucose uptake rate dramatically increases, and lactate is generated. This process, known as the Warburg Effect, has been documented for over 90 years [41].

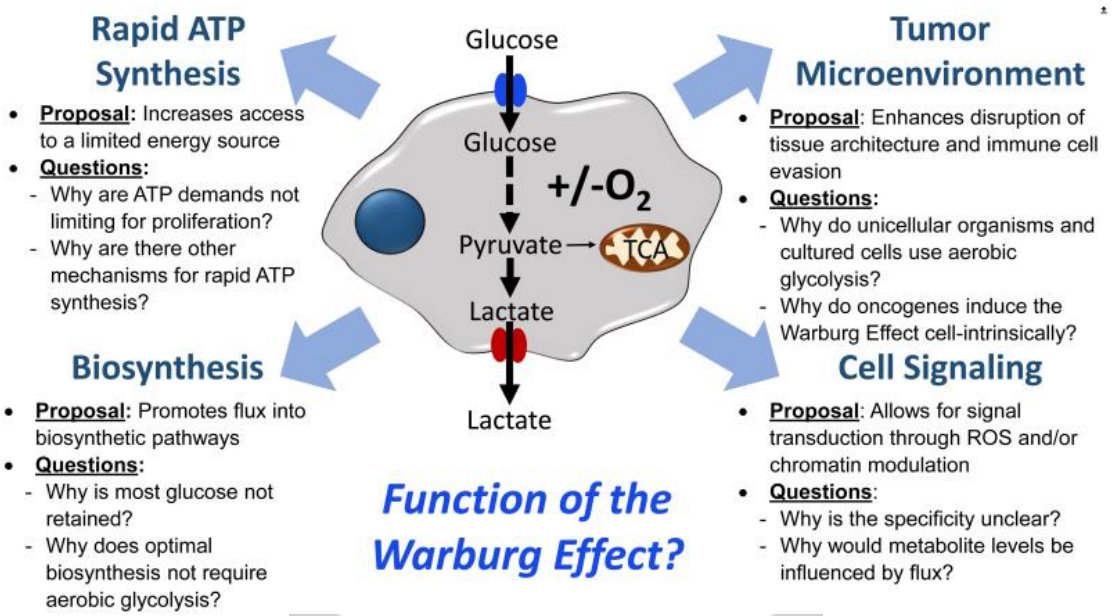

Figure 1.6 An increase in the rate of glucose and favorable production of lactate uptake even in the presence of oxygen is defined as the Warburg Effect [41].

Several functions have been hypothesized the Warburg Effect as Fig. 1.6 shown, and these functions of the Warburg Effect for tumor growth even today remain unknown. In general, literature values of pH in the tumor area ranges from 6.5 to 7.0 [42]. Since tumoral microenvironment is slightly acidic, this property can be applied to nanoparticle delivery.

1.4 Experiment design

1.4.1 Tumor targeting *via* cancerous pH-responsive ethylenediamine-

based polycarboxybetaine

We previously reported an ethylenediamine-based polycarboxybetaine zwitterion [PGlu(DET-Car)] in 2018 which demonstrated enhanced tumor accumulation through its pH-regulated switch to net cationic, occurring selectively within acidic tumor tissue as well as prolonged blood circulation owing to its anti-fouling behavior [43] (Fig. 1.7). The two distinct pK_a values of the ethylenediamine group in PGlu(DET-Car) side chains were confirmed to be around 6.3 and 9.0 [43], which is able to maintain net neutral charge at physiological pH (7.4) and protonate at cancerous pH (6.5).

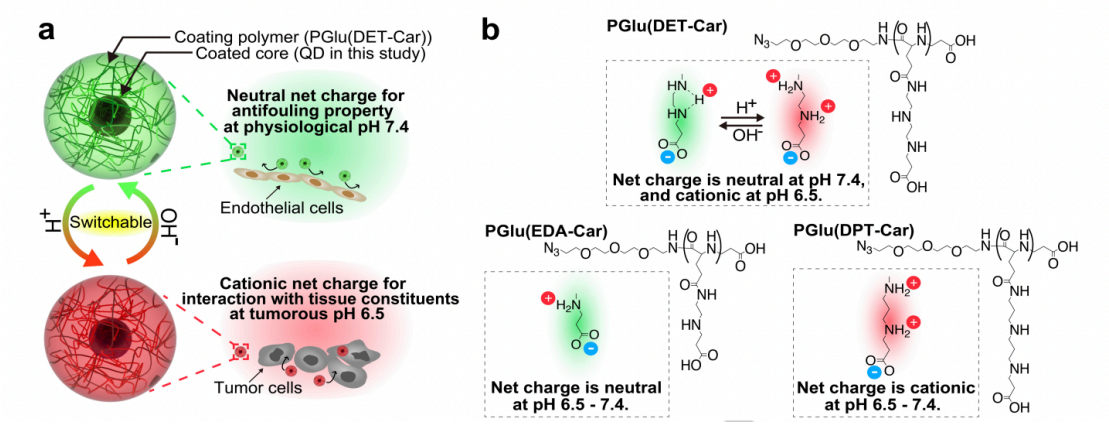

Figure 1.7 Charge switch property and protonated structure of the side chain in PGlu(DET-Car) [43].

In this research, we corroborated these pK_a properties in siRNA-encapsulated LNP, where they were determined to be near-neutral at

physiological pH (7.4) and switch to cationic at cancerous pH (6.5). As mentioned in chapter 1.2.1, neutrally charged nanoparticles possess longer circulation than cationic particles which facilitate cellular uptake through interaction with anionic cell membrane.

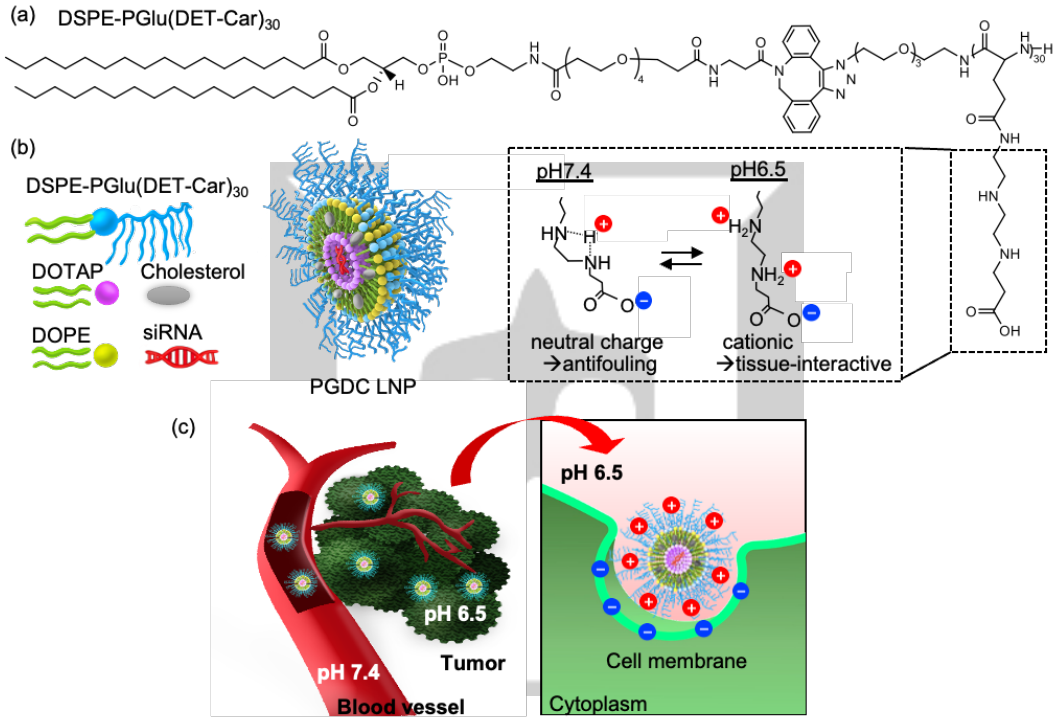

Figure 1.8 PGlu(DET-Car) modified LNP. (A) Structure of DSPE-PGlu(DET-Car)$_{30}$, (B) Schematic illustration of siRNA-encapsulated PGlu(DET-Car)$_{30}$ LNPs, (C) How PGlu(DET-Car)$_{30}$ LNPs facilitate tumor accumulation through pH switchable property.

As Fig. 1.8 showed, the LNP surface charge was designed to be near neutral in physiological pH, and switch to positive *via* bisprotonation of the polycarboxybetaine ethylenediamine moiety in the reduced pH. Moreover, as

mentioned in 1.2.1, hydrophilic property of polyzwitterion helps to hinder protein adsorption of MPS clearance, which was expected to prolong the circulation time and further facilitate tumor accumulation.

1.4.2 Endosomal escape

The use of pH-sensitive ionizable lipids which can be designed to exploit the differences in pH observed between physiological and tumorous pH is able to enhance tumor targeting [44].

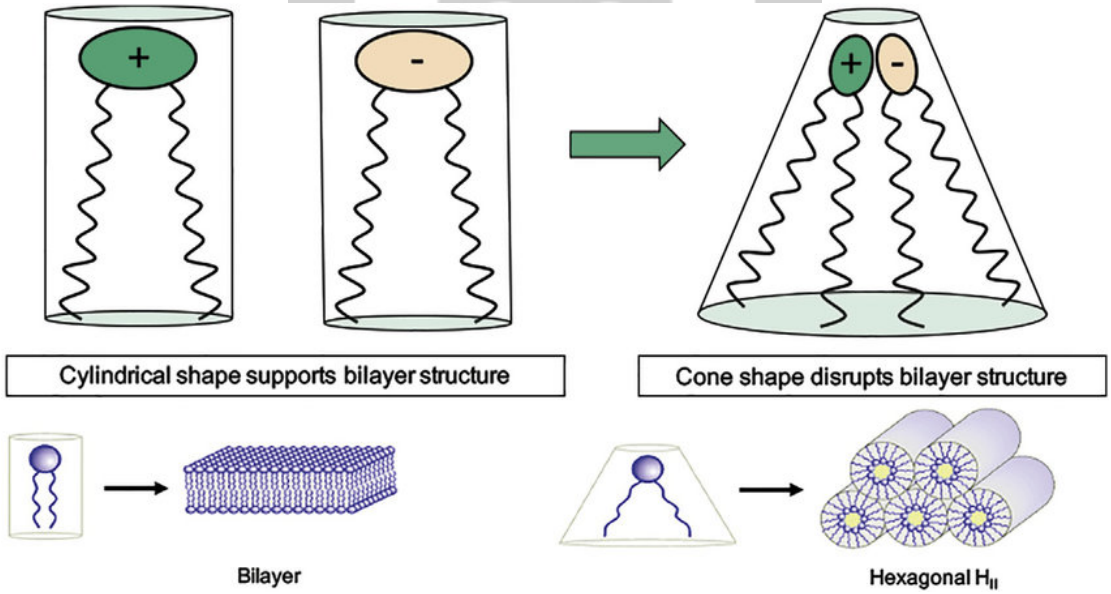

Figure 1.9 Mechanism of membrane disruptive effects of cationic lipids in endosome [45].

Similarly, ionizable lipids with a pKa < 6.5 are regularly utilized to improve endosomal escape *via* head group protonation within the acidic environment of

endosomes [44, 46]. As Fig. 1.9 showed, cationic lipids of LNP and anionic lipids present in the endosome adopt a cylindrical molecular shape. When cationic and anionic lipids are close together, ion pairs which are formed through the lipid combination adopt a cone molecular shape promoting the formation of non-bilayer phase which is associated with membrane disruption. Therefore, the positively charged surface of LNP owing to protonation of ethylenediamine moiety in response to acidic pH in the endosomal compartment enables electrostatic interaction with the endosomal membrane, allowing enhanced endosomal escape of siRNA through the membrane fusion mechanism.

In 2020, application of ethylenediamine-based polycarboxybetaine to MRI contract agent was reported to showed tumor-specific activatable T_2 MRI contrasting enhancement [47]. PGlu(DET-Car) is a one of the most promising polyzwitterion-based materials for enhanced tumor accumulation. This is the first instance of ethylenediamine-based polycarboxybetaine-modified LNP having cancerous pH-responsivity demonstrating siRNA delivery *in vitro* and *in vivo*.

Chapter 2 Synthesis of polyzwitterion modified lipid

2.1 Introduction

Synthesis methods of N_3-PGlu(DET-CAR)$_{30}$ was described in previous research [43]. The polyzwitterion PGlu(DET-CAR)$_{30}$ contains an azido group, therefore, could be conjugated with dibenzocyclooctyne (DBCO)-bearing reagents through click chemistry as Fig. 2.1 showed [48, 49] without removing metal ions during reaction.

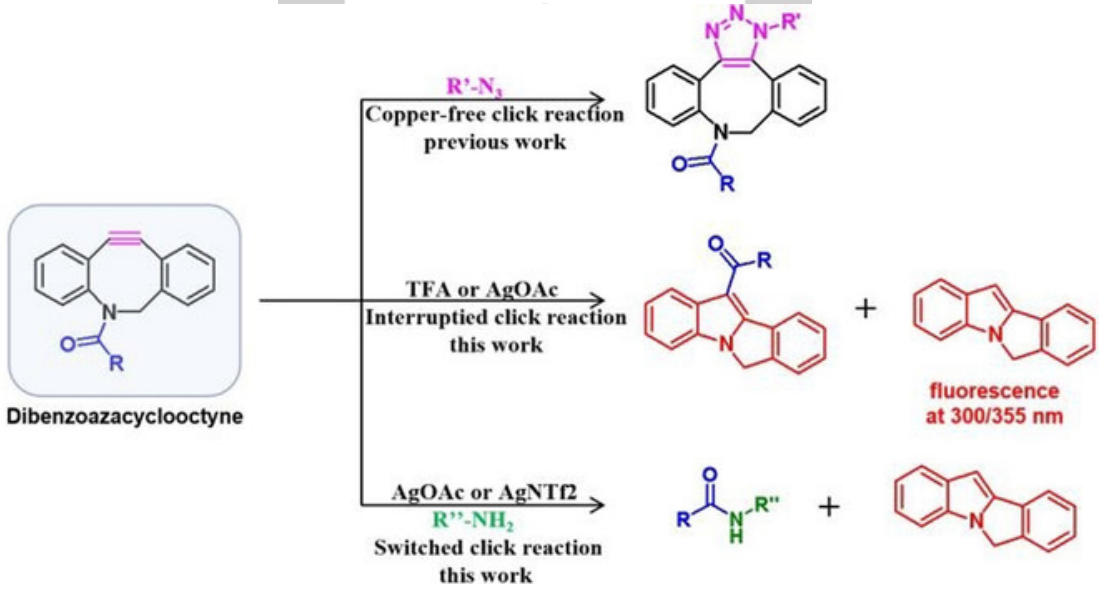

Figure 2.1 Click reactivity of DBCO under different conditions [49].

DSPE-PEG4-DBCO is a commercial 1,2-Distearoyl-sn-glycero-3-phosphorylethanolamine (DSPE) product containing DBCO moiety with PEG linker and phospholipid DSPE. Hence, DSPE-PEG4-DBCO was used to

prepare polyzwitterion modified lipid by conjugating to N_3-PGlu(DET-CAR)$_{30}$.

2.2 Materials and methods

Hydrophilic PGlu(DET-CAR)$_{30}$ was dissolved in water (0.074 mmol) and DSPE-PEG$_4$-DBCO was dissolved in dichloromethane (DCM) (0.111 mmol) followed by 48 h mixing at room temperature (r.t.). Next, unreacted DSPE-PEG$_4$-DBCO was removed by recrystallization with excess acetonitrile (AcN) for one day stirring. After discarding the supernatant, residue was washed with AcN and solvent was removed by centrifugation followed by decantation. The final product was obtained *in vacuo* (98% yield). The yield of DSPE-PGlu(DET-CAR)$_{30}$ was estimated to be *ca.* 87% evaluated by high performance liquid chromatography (HPLC) with 40% tetrahydrofuran (THF) of mobile phase. The chemical structure was confirmed by ^{1}H NMR analysis using 0.65% deuterium chloride (DCl) in deuterium oxide (D_2O) at r.t. (Fig. 2.2).

2.3. Results and discussion

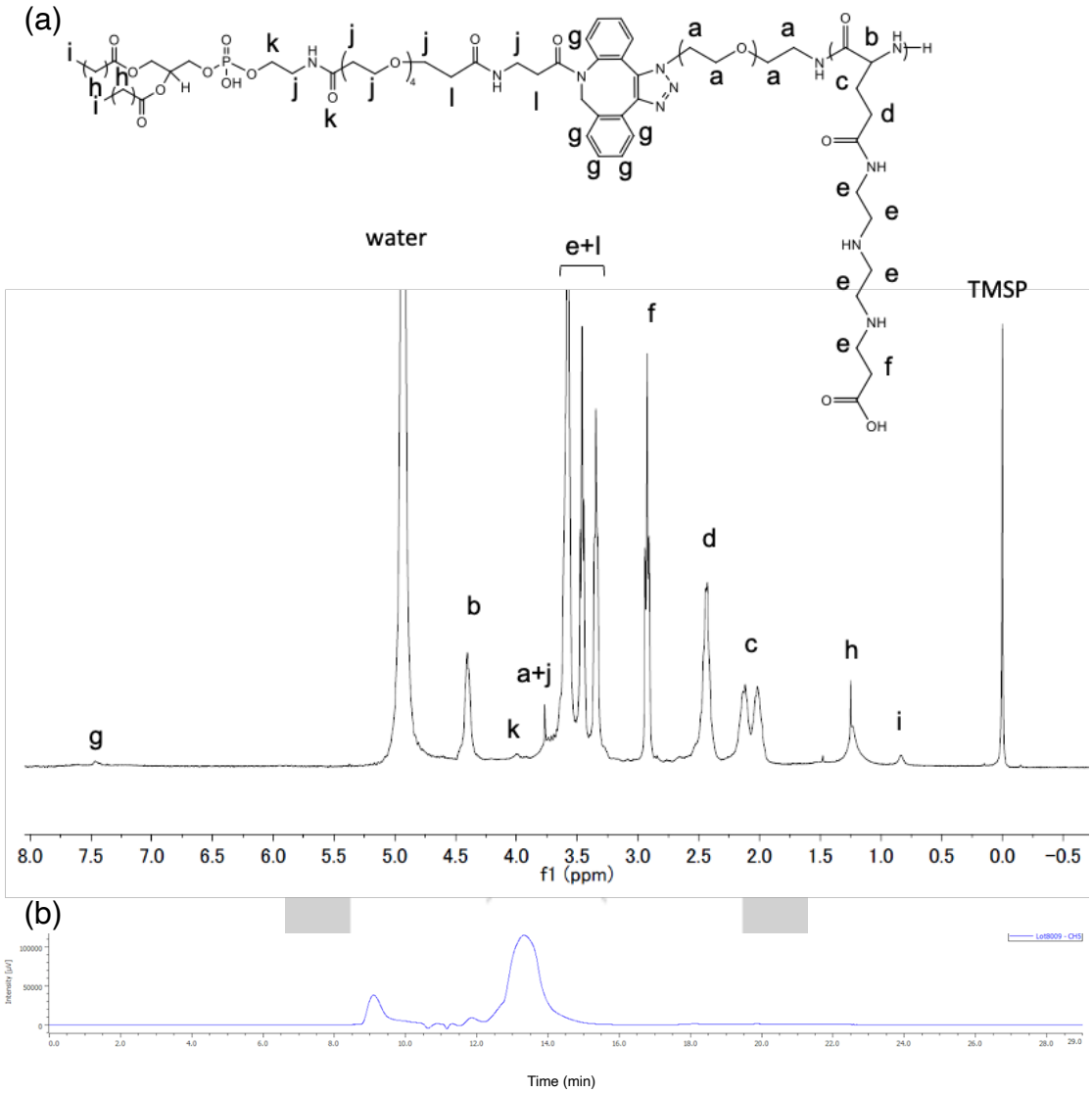

Figure 2.2 Analysis of DSPE-PGlu(DET-Car)$_{30}$. (a) ^{1}H NMR spectrum of PGlu(DET-Car) phospholipid and (b) HPLC data.

As Fig. 2.2 (a) showed, each carbon had its corresponding peak and integral value (not shown) in NMR spectrum including the DBCO moiety as well as long carbon chain of lipid tails. In HPLC analysis, peptide bonds absorb light strongly generally at 210–220 nm [50]. Fig. 2.2 (b) showed the absorbance peak at 220

nm indicating the DET-Car moiety of the DSPE-PGlu(DET-CAR)$_{30}$. The DSPE-PGlu(DET-CAR)$_{30}$ contained hydrophobic lipid tails, therefore its peak (13.5 min) came after N_3-PGlu(DET-CAR)$_{30}$ (9 min), and the yield calculated by the integral of its area was about 87%. The ^{1}H NMR spectrum together with HPLC data suggested the successful synthesis of DSPE-PGlu(DET-CAR)$_{30}$.

Chapter 3 Preparation/characterization of lipid nanoparticles

3.1 Preparation of lipid nanoparticles

3.1.1 Introduction

3.1.1.1 Helper lipids

LNPs are thought to be a safer vector owing to similar composition of cell membrane. To form LNPs, helper lipids play an important role to stabilize LNP and contribute to deliver efficiency [51]. Phospholipids are the most used as helper lipids such as distearoylphosphatidylcholine (DSPC), 1,2-dioleoyl-sn-glycero-3-phosphocholine (DOPC), 1,2-Distearoyl-sn-glycero-3-phosphorylethanolamine (DSPE) and 1,2-dioleoyl-sn-glycero-3-phosphoethanolamine (DOPE) (Table 3.1). Phosphatidylethanolamines (PE) are found in all living cells [52]. Helper lipids containing double bond might

facilitate membrane fusion process [53, 54].

Table 3.1 Chemical structure of phospholipids

Phosphocholines	
DSPC	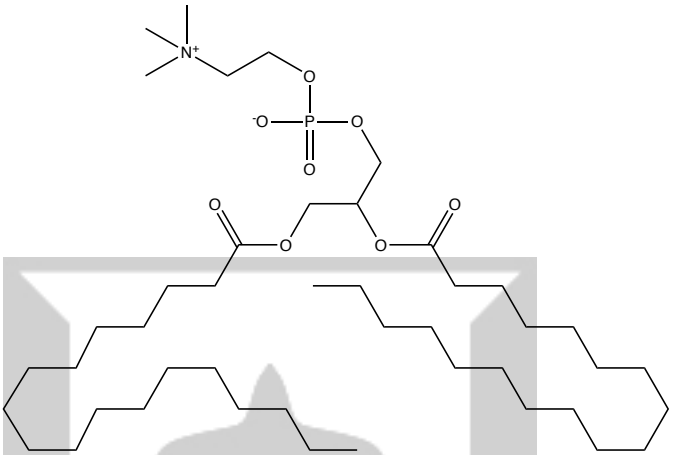
DOPC	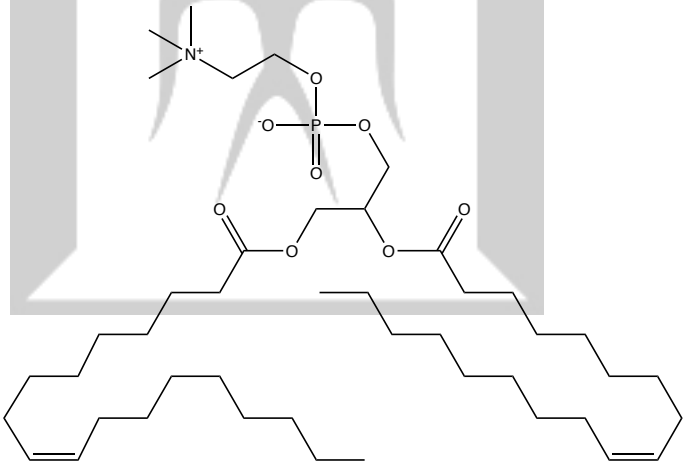
Phosphatidylethanolamines	
DSPE	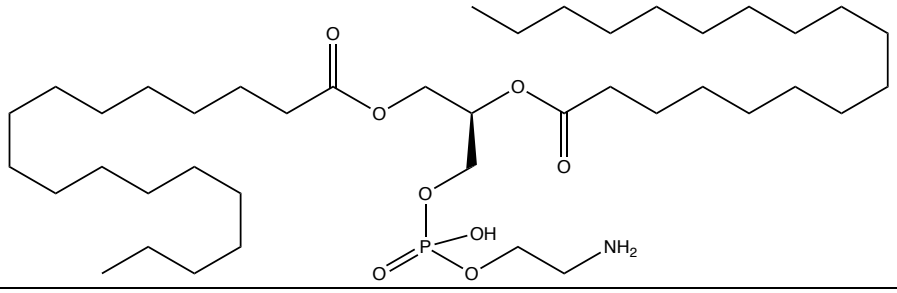

DOPE	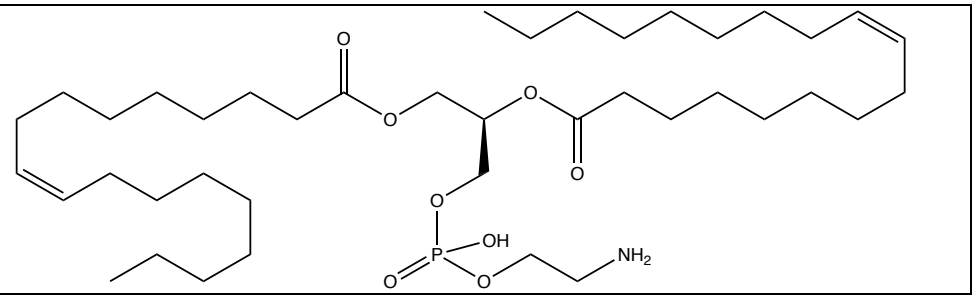

Therefore, we used DOPE as helper lipid. Beside phospholipids, cholesterol is a crucial neutral helper lipid that influents the fluidity and contributes to stability [55]. The presence of cholesterol decreases the fluidity of LNP and therefore increase the stability of LNP.

3.1.1.2 Cationic lipids for siRNA encapsulation

Cationic lipids are used to electrostatically interact with negatively charged nucleic acids (Table 3.2) for nucleic acid delivery. 1,2-dioleoyl-3-trimethylammonium-propane (DOTAP) which is one of the most widely used cationic lipids is completely protonated at pH 7.4 [56].

Table 3.2 Chemical structure of cationic lipids for siRNA encapsulation

DOTAP	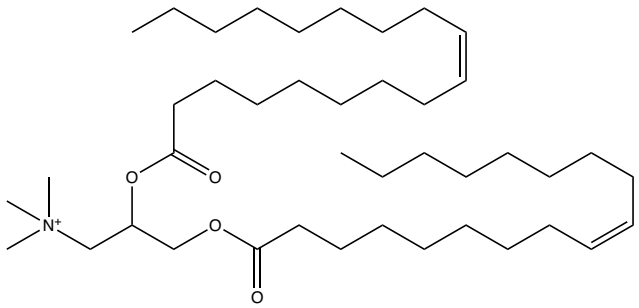
DODAP	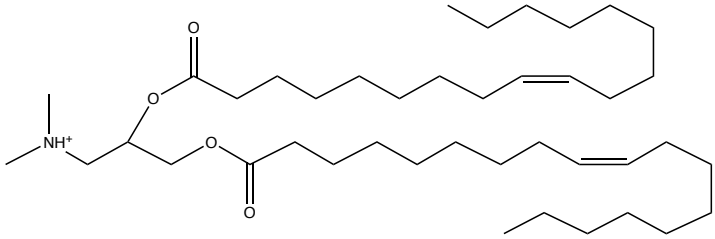

1,2-dioleoyl-3-dimethyaminopropane (DODAP) which has a *pKa* about 5.8 [16] is an ionizable lipid used in nucleic acid encapsulation [57]. Given that pH in the tumor area ranges from 6.5–7.0 [40], both DODAP and our polyzwitterion [PGlu(DET-Car)] would be protonated in response to the acidic tumoral pH. In order to assess whether PGlu(DET-Car) modified LNP could enhance tumor targeting and siRNA delivery efficiency, we used DOTAP to encapsulate siRNA to avoid the interference from the ionizable lipid DODAP.

3.1.2 Materials and methods

siRNA-loaded PGlu(DET-CAR)$_{30}$ LNPs were prepared according to the tert-butanol (*t*-BuOH) dilution procedure employed by Sato et al [58]. Briefly, hydrophobic materials: DOPE, cholesterol and DOTAP in varying compositions

were dissolved in 200 μL of 90% *t*-BuOH solution. Separately, aqueous solutions of DSPE-PGlu(DET-Car)$_{30}$ in various concentrations were each mixed with 20 μL 1 mg/mL siRNA buffered in pH 7.4 4-(2-hydroxyethyl)-1-piperazineethanesulfonic acid (HEPES), and the contents thoroughly mixed. The lipid mixtures were then added into HEPES buffer under vigorous stirring to facilitate formation of LNPs. *t*-BuOH was replaced by consecutive dilutions with phosphate buffered saline, (D-PBS(-) or PBS) followed by ultrafiltration. siRNA-loaded PEGylated LNPs or PEG LNPs were prepared as a control following the methods outlined above with N-(Methylpolyoxyethylene oxycarbonyl)-1,2-distearoyl-sn-glycero-3-phosphoethanolamine (DSPE-PEG$_{5k}$) (Fig. 3.1). Although DSPE-PEG$_{5k}$ and DSPE-PEG$_{2k}$ were 2 commonly commercial PEGylated lipids, the molecule weight of PEG$_{5k}$ is much closer to PGlu(DET-Car)$_{30}$ than PEG$_{2k}$, therefore, DSPE-PEG$_{5k}$ was used as surface modification material of control LNP.

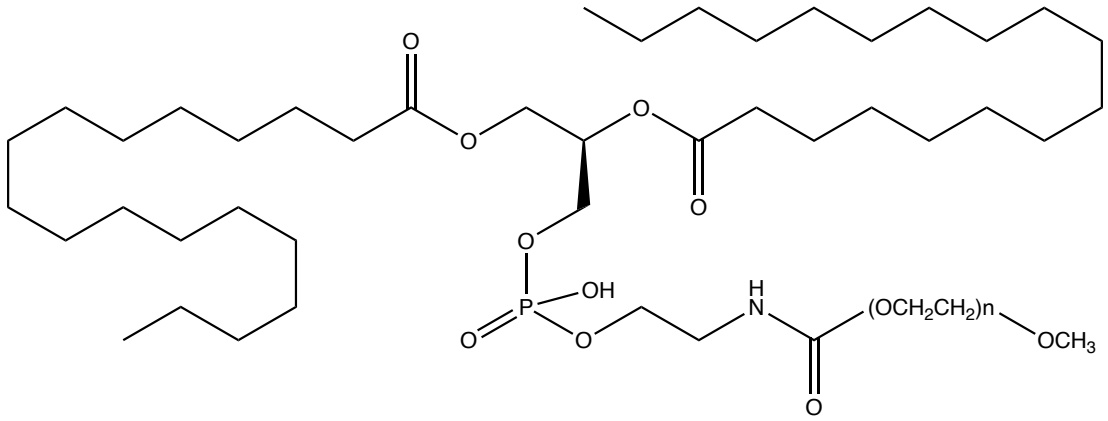

Figure 3.1 Chemical structure of DSPE-PEG5k

3.1.3 Results and discussion

Considering protonated polyzwitterion might affect the siRNA encapsulation, lipid materials were mixed in HEPES buffer (pH 7.4) rather than acidic pH in which other methods prepare LNPs for effective encapsulation of cationic lipid and nucleic acids. Lipid solution is often lyophilized and hydrated in conventional methods. In this study, solvent was replaced with PBS during ultrafiltration, and consequently, LNPs dissolved in PBS can be directedly and immediately used in *in vitro* and *in vivo* experiments. LNPs were evaluated by a Zetasizer. Characterization results of LNPs was discussed in chapter 3.2.

3.2 Characterization of lipid nanoparticles

3.2.1 Introduction

Blood circulation of nanoparticle is influenced by such as particle shape, size and surface potential. First, particle size < 200 nm is small enough to leak to tumor *via* EPR effect and > 150 nm tends to accumulate in spleen and liver [18, 33, 59]. Therefore, size optimization of LNP is important for improved blood circulation time. In addition, the presence of high protein concentration may cause fracture or shrinkage of LNP structure [60, 61]. Hence, stability in serum is a crucial factor to make sure LNP would not be easily destroyed during circulation. Hydrodynamic diameter and size distribution of LNP were determined through monitoring Brownian Motion by dynamic laser scanning (DLS) in a Zetasizer. Serum stability was observed by size change within 48 h incubated in serum at 37°C.

Stepwise protonation behavior of PGlu(DET-Car) in acidic cancerous pH leads to great change of surface charge from neutrality to positiveness. To evaluate the pH-responsive ability of LNPs, the ζ-potential of LNPs was determined through the electrophoretic mobility of the particles by laser doppler velocimetry in a Zetasizer.

To assess whether siRNA was well-encapsulated in the LNPs, we used

RiboGreen® RNA reagent which is non-fluorescent when free in solution. Upon binding siRNA, the RNA bound RiboGreen® reagent would have an excitation ~500nm and an emission ~525nm which can be detected by a microreader.

3.2.2 Materials and methods

3.2.2.1 Characterization of siRNA-loaded LNPs

Hydrodynamic size, polydispersity (PDI), and ζ-potential of LNPs were determined using a Zetasizer. Size change with time in serum was evaluated through dispersing LNP in 50% fetal bovine serum (FBS) followed by incubation for 48 h in an incubator (37 °C, 5% CO_2, 95% humidity). The morphology of LNP was observed using a transmission electron microscopy (TEM).

3.2.2.2 Encapsulated Efficiency (EE%)

siRNA encapsulation efficiency was determined by RNA quantification using the RiboGreen assay according to the manufacturer's instructions. For determination of total siRNA, Quant-iT™ RiboGreen® RNA reagent was diluted with HEPES buffer (pH 7.4) containing 0.4% (*v/v*) Triton X-100 and 80 μg/mL dextran sulfate to form lysis buffer. This was subsequently mixed with the LNP

solution. For free siRNA determination, Quant-iT™ RiboGreen® RNA reagent was diluted with HEPES buffer (pH 7.4) and mixed with the LNP solution. The fluorescence of total and free siRNA was measured using a microplate reader (Ex: 480 nm, Em: 525nm). Separate calibration curves were constructed for each solution to account for the effects of Triton X-100 and dextran sulfate on fluorescence intensities. EE % was determined by the following equation.

$$EE\ (\%) = ([total\ siRNA – free\ siRNA] / total\ siRNA) \times 100\%$$

3.2.2.3 ζ-potential

ζ-potential of LNPs was measured using a Zetasizer when LNP dispersed in acetate buffer (pH 5.5), 2-(*N*-morpholino)ethanesulfonic acid (MES) buffer (pH 6.5), and HEPES buffer (pH 7.4).

3.2.3 Results and discussion

3.2.3.1 Particle size and serum stability

DOTAP, DOPE, cholesterol and DSPE-PGlu(DET-CAR)$_{30}$ at different composition were used to prepare siRNA-loaded DSPE-PGlu(DET-CAR)$_{30}$ modified LNPs (Table 3.3). To evaluate the pH-responsiveness of PGlu(DET-

CAR)$_{30}$ LNP, polyzwitterion modified LNP, we prepared the control LNP using commercial PEG lipid as mentioned in chapter 3.1.2. The control LNP was designed to have similar size as PGlu(DET-CAR)$_{30}$ LNP using DOPE / cholesterol / DOTAP / DSPE-PEG5k (34% / 29% / 34% / 3%). The size distribution by intensity (Fig. 3.2 a) and average hydrodynamic diameter (Fig. 3.2 b) of PGlu(DET-Car) LNP and control LNP are both 130 nm which is suitable for tumor delivery *via* EPR effect.

Table 3.3 Characteristic of PGlu(DET-CAR)$_{30}$ LNPs through different lipid composition with various molar ratios using DLS.

Lipid Composition (%)				Diameter [a)]	PDI [a)]
DOTAP	DOPE	Cholesterol	PGlu(DET-CAR)$_{30}$		
30	40	30	1	290 ± 1.3	0.199 ± 0.037
40	30	30	1	270 ± 0.2	0.180 ± 0.001
35	35	30	1	220 ± 2.0	0.144 ± 0.036
34	34	30	2	160 ± 1.4	0.165 ± 0.016
34	34	29	3	140 ± 0.1	0.195 ± 0.003
32	32	28	7	130 ± 0.7	0.275 ± 0.004

[a)] Determined by DLS

We found that increased DSPE-PGlu(DET-CAR)$_{30}$ ratio helps to formed smaller LNPs (Table 3.3). The optimized LNP containing 7% DSPE-PGlu(DET-CAR)$_{30}$ has a size of 130 nm which is suitable for passive accumulation into tumor

tissues *via* EPR effect while reducing high accumulation in spleen and liver *via* MPS clearance as mentioned in chapter 3.2.1.

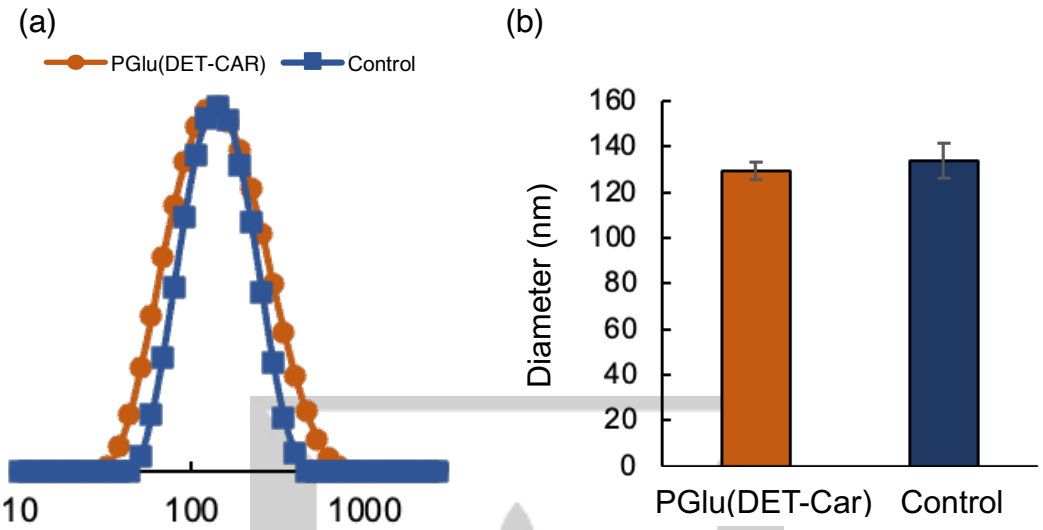

Figure 3.2 Characterization of siRNA-loaded PGlu(DET-CAR)$_{30}$ LNP and control LNP. (a) Size distribution by intensity. (b) Hydrodynamic diameter (n=10).

The morphology of LNPs was carried out by TEM as Fig. 3.3 showed. LNPs had spherical shape, and the size of LNPs observed in TEM image was slightly smaller than measured by DLS (Fig. 3.2) owing to the dehydration process in sample preparation.

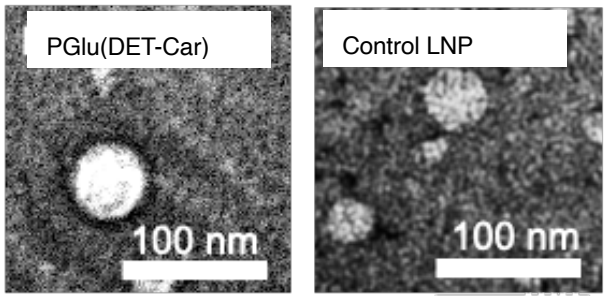

Figure 3.3 TEM image of LNP.

In conventional PEGylated LNP, PEG chains interact strongly with water molecules to form a hydration layer which can strengthen colloid stability and avoid protein adsorption [62, 63]. Besides, LNP size is predominantly controlled through modifying the molar ratio of PEG-lipid in formulation, as well as adjusting the chain length of individual PEG molecules [64]. Increased PEG lipid ratio results in reduction of LNP size [64]. We found that the size of PGlu(DET-CAR)$_{30}$ LNPs was analogously controllable *via* differing ratios of PGlu(DET-Car)$_{30}$ (Table 3.3).

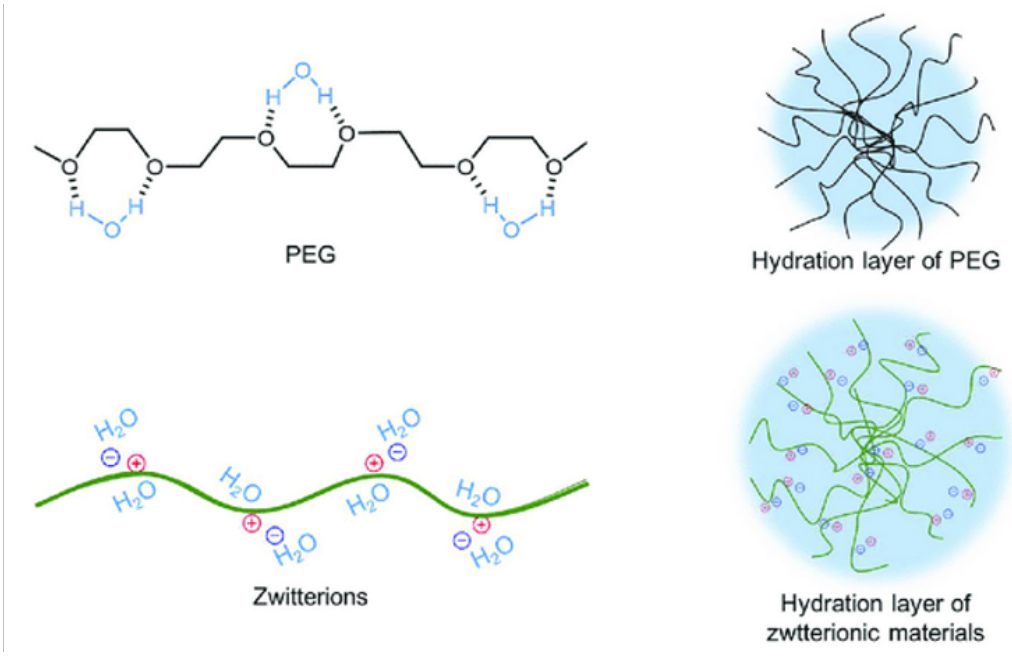

Figure 3.4 Hydration layer formed by PEG and polyzwitterion [65].

The formulation of PGlu(DET-CAR)$_{30}$ LNPs and control LNPs were comparable, and the obtained LNPs had analogous size; in addition, the size tuning was also available by changing mixing ratio of DSPE-PGlu(DET-Car)$_{30}$, suggesting the facile preparation of PGlu(DET-CAR)$_{30}$ LNPs similar to conventional control LNPs. As showed in Fig. 3.4, This may result from the formation of hydration layer owing to the interaction between water molecules and zwitterions [65]. Therefore, in this system, LNP size is controllable through adjusting the proportion of DSPE-PGlu(DET-CAR)$_{30}$.

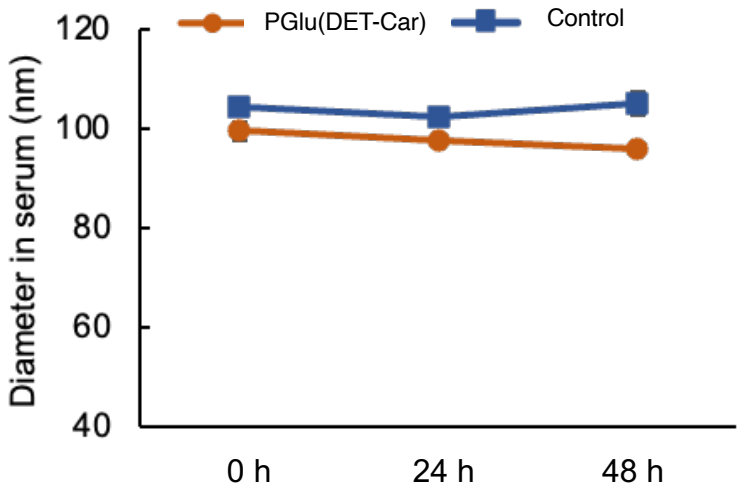

Figure 3.5 Hydrodynamic change as time in the presence of serum (n=3).

In real blood circulation, high protein concentration is possible to disturb LNP structure and reduce its stability [60, 61]. To evaluate whether LNP was stable in the presence of serum, we examined the size change for 48 h in high concentration of serum. The size of LNP would become a bit smaller in serum (100 nm) than in PBS (130 nm) (Fig. 3.2 and 3.5) because of the osmotic pressure [60]. As Fig. 3.5 showed, both PGlu(DET-CAR)$_{30}$ LNP and control LNP had little change in size indicating that these LNPs were stable in the presence of serum.

3.2.3.2 Encapsulated efficiency

EE% were determined by RiboGreen assay. As Fig. 3.6 showed, PGlu(DET-CAR)$_{30}$ LNP as well as control LNP possessed high EE% (> 90%)

suggesting that siRNA was well encapsulated in LNPs *via* interaction with cationic lipid DOTAP.

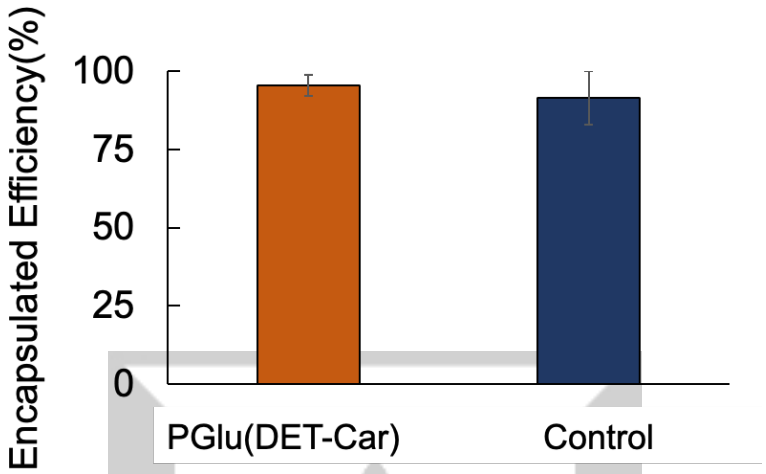

Figure 3.6 Encapsulated efficiency of LNPs determined by RiboGreen assay (n=10)

The high siRNA encapsulation efficiency resulted from sufficient DOTAP with the ratio of positively chargeable polymer amine groups to negatively charged nucleic acid phosphate groups (ratio of N/P) 4.

3.2.3.3 ζ-potential

ζ-potential of LNPs were examined after confirming both PGlu(DET-CAR)$_{30}$ LNP and PEGylated control LNP having similar size, serum stability and same high EE%. As Fig. 3.7 showed, PGlu(DET-CAR)$_{30}$ LNP was close to neutral at

pH 7.4, and switch to highly positive charge at pH 6.5 and 5.5 while control LNP showed little change. This increased ζ-potential of PGlu(DET-CAR)$_{30}$ LNPs should be owing to bisprotonation of the ethylenediamine moieties of PGlu(DET-Car) (Fig. 1.8).

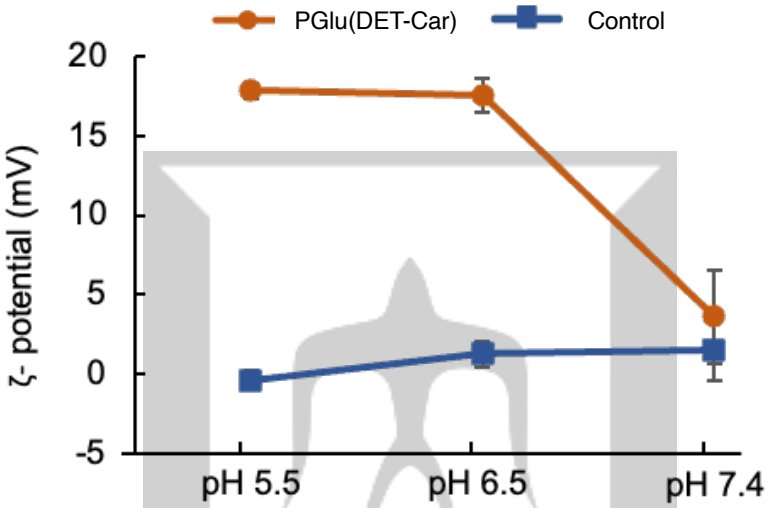

Figure 3.7 ζ-potential of LNPs at pH 5.5, 6.5 and 7.4.

Given the pH of the tumor microenvironment is about pH 6.5 and pH of endosome is about 5.5 [36, 66, 67], PGlu(DET-CAR)$_{30}$ LNPs are expected to exert the facilitated cellular uptake and endosomal escape in response to acidic pH.

Chapter 4 *In vitro* assessment

4.1 Cellular uptake

4.1.1 Introduction

In the previous chapter, pH-responsive and charge-switchable property of PGlu(DET-CAR)$_{30}$ LNP resulted from protonation of amino group was confirmed. In this chapter, *in vitro* assessment was conducted to evaluate the pH-dependent behaviors using cancer cell lines. We evaluated tumoral pH-dependent cellular uptake of PGlu(DET-CAR)$_{30}$ LNPs compared with PEGylated control LNP.

Alexa647 which is a commercial pH-insensitive far-red–fluorescent dye is ideal for flow cytometry and stable signal generation in imaging. Moreover, the excitation wavelength of Alexa647 differs from RiboGreen, which avoid inaccurate quantification of EE%. LNPs encapsulating Alexa647-labeld siRNA were used to estimate whether siRNA-loaded LNPs were internalized.

4.1.2 Materials and methods

Murine colon cancer cells (CT26) and human ovarian carcinoma cells expressing the firefly luciferase gene (SKOV3-luc) were sub-cultured in

Dulbecco's Modified Eagle Medium (DMEM) with 10% FBS and 1% penicillin and were maintained at 37 °C in an incubator (5% CO_2, 95% humidified environment).

Cells were seeded in a 24-well plate (5×10^4 cells/well). pH 6.5 DMEM was prepared by addition of diluted hydrochloric acid (HCl) at 37 °C followed by filtration with a 0.22 μM filter. After a 24 h incubation, the culture media was replaced with fresh media (pH 7.4 and 6.5) containing fluorescence labeled siRNA (Alexa647-siGL3)-loaded LNPs at a final concentration of 100 nM siRNA, followed by an additional 6 h incubation. Subsequently, cells were washed twice using PBS, detached with trypsin/EDTA, and suspended in media. The fluorescence intensity of cells was measured by a flow cytometer (FCM) (Ex: 642 nm, Em: 661 nm).

The values are expressed as the mean ± standard deviation (SD). Statistical analysis was conducted using Student's *t*-test. A p value of < 0.05 was considered statistically significant.

4.1.3 Results and discussion

We examined the cellular uptake of this newly tumoral pH-responsive surface modification onto LNP, in cancerous acidic pH through co-incubation of

CT26 or SKOV3-luc cell line with PGlu(DET-Car) LNP for 2 h and 6 h at pH 6.5 and pH 7.4 medium.

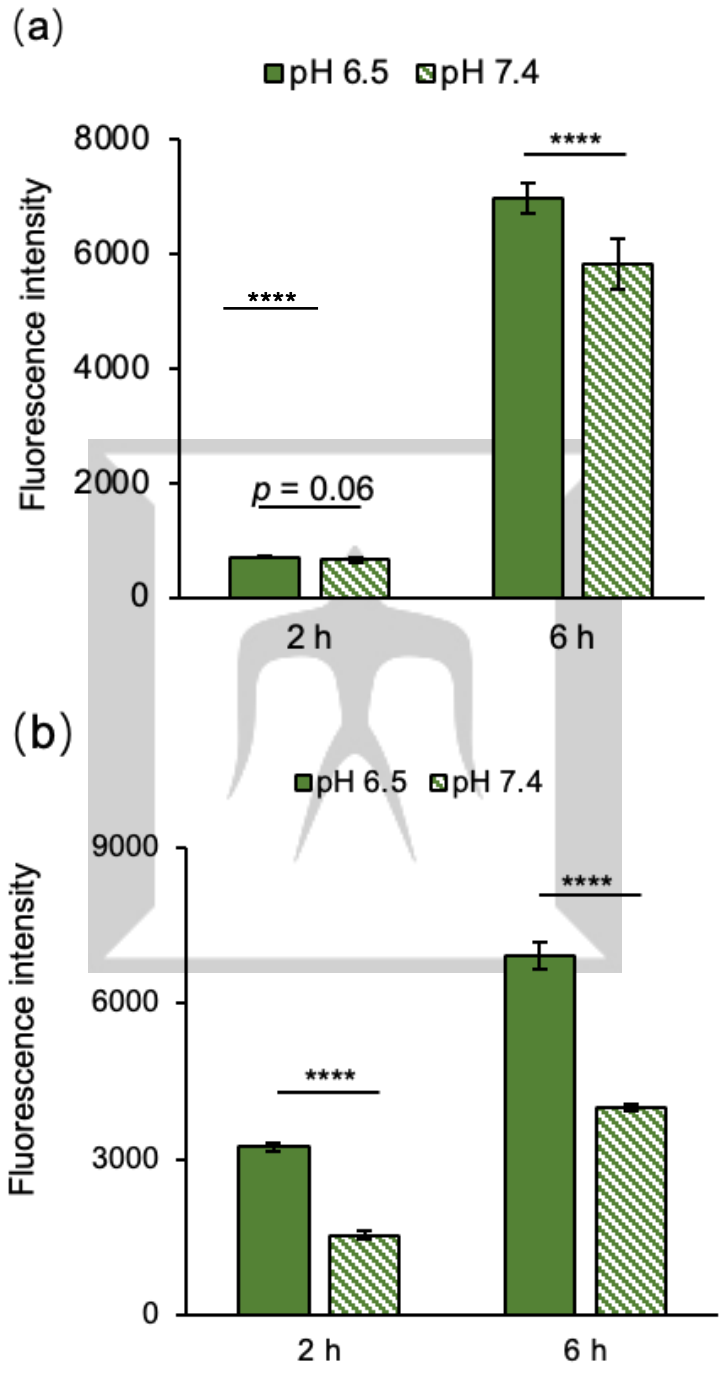

Figure 4.1 Cellular uptake of PGlu(DET-Car) LNP at pH 6.5 and 7.4. 2 h and 6 h incubation of Alexa647-siGL3 loaded PGlu(DET-Car) LNP with (a) SKOV3-luc and (b) CT26 cells.

As Fig. 4.1 showed, the fluorescence intensity (FI) of PGlu(DET-Car) LNP in 6 h is higher than 2 h, which indicated that the time-dependent cellular uptake of PGlu(DET-Car) LNP. Furthermore, PGlu(DET-Car) LNP expressed significantly higher cellular uptake at pH 6.5 than pH 7.4 as Fig. 4.1 showed, which suggested that acidic pH-responsive property of PGlu(DET-Car) improved cellular uptake in cancerous environment (pH 6.5).

The change in surface charge to cationic at tumoral pH 6.5 of PGlu(DET-Car) LNP contributed to the observed increase in cellular uptake owing to the facilitated interaction between positively charged PGlu(DET-Car) LNP and negatively charged cell membrane. PGlu(DET-Car) LNP demonstrated significantly higher cellular uptake at pH 6.5 compared to pH 7.4 (Fig. 4.1). These results confirmed the cancerous pH-responsivity of PGlu(DET-Car) LNP even in protein-enriched biological conditions.

4.2 Endosomal escape

4.2.1 Introduction

After confirming successful cellular uptake of LNPs and pH-dependent uptake property of PGlu(DET-CAR)$_{30}$ LNPs, we examined the endosomal escape through subcellular distribution of LNPs by confocal laser scanning

microscope (CLSM) images.

As described in chapter 1.1.1, siRNA needs to be released from vectors and then is able to recognize target mRNA. Beside the Alexa647 which is used to label siRNA, Hoechst 33342 which tends to bind to adenine–thymine-rich regions of DNA was used to distinguish condensed pycnotic nuclei. LysoTracker® probes are highly selective for acidic organelles such as endosomes and lysosomes, therefore were used to label endosomes. Endosomal escape was examined *via* colocalization of LysoTracker-stained organelles and Alexa647-siRNA. Colocalization can be explained as an existence of the signal at the same pixel location when examining multichannel fluorescence CLSM images [68]. Colocalization is typically shown by presenting a plate of three images consisting of green and red channels as well as a merged image where the channels are combined and overlapping pixels turn yellow. Note, it is estimated that less than 2% of the siRNA administered *via* LNPs escapes the endosomes to reach the cytosol [69, 70]. In addition, the fluorescence intensity of free Alexa647-siRNA is too week to see, but the fluorescence intensity of concentrated Alexa647-siRNA encapsulated inside LNPs can be observed in CLSM images. Indeed, endosomal escape assessment is difficult to determine. The efficiency of encapsulated siRNA

release from endosome was compared through colocalization ratio change with time. Generally, a major proportion of LNPs is endocytosed by cells in about half hour [69, 70]. Hence, we compared the colocalization ratio of Alexa647-siRNA with LysoTracker-labeled organelles at time point 1 h and 8 h.

To further examine endosomal escape, LNPs were co-incubated with calcein for 1.5 h. Calcein is a small membrane-impermeable dye which looks punctate when sequestered within endosomal/lysosomal compartments [71] and taken up by cells through endocytosis [72]. If calcein was uptaken, it could not pass through the plasma membrane. On the other hand, when calcein was released from endosome, it appears diffused green color in the whole cytosol. The diffusion of calcein into the cytosol represents the disruption of the endosomal membrane.

4.2.2 Materials and methods

4.2.2.1 Co-localization of siRNA in endosome/lysosome

CT26 cells (1×10^5 cells/dish) and SKOV3-luc (5×10^5 cells/dish) were seeded in 35-mm glass dishes with DMEM containing 10% FBS and 1% penicillin for 24 h incubation. The cells were treated with fresh media at pH 6.5 containing Alexa647-siGL3-loaded LNPs at a final concentration of 100 nM

siRNA, followed by an additional 1 h and 8 h incubation. The cells were subsequently washed twice using PBS. The cells were stained by LysoTracker® Red DND-99 (50 nM) for 30 min and by Hoechst33342 (10 μg/mL) for 5 min. The cells were washed with PBS twice after each staining step and were then observed using a confocal laser scanning microscope (CLSM) at excitation wavelengths 405 nm for Hoechst33342, 561 nm for Lysotracker Red DND-99 and 633 nm for Alexa-647 siRNA-loaded LNPs. The co-localization ratio was calculated by ZEN software for LSM710.

4.2.2.2 Calcein release assay

SKOV3-luc and CT26 cells were seeded overnight at a density of 5,000 cells/well in DMEM containing 10% FBS and 1% penicillin in Lab-Tek® Chambered #1.0 Borosilicate Coverglass wells. Cells were washed using PBS, and media were replaced with fresh media (pH 6.5) containing 250 μM calcein and Alexa647-siGL3-loaded LNPs at an siRNA dose of 100 nM, followed by 1.5 h-incubation. Endosomal escape of LNPs was observed in DMEM using a CLSM at excitation wavelengths 405 nm for Hoechst33342 and 488 nm for calcein.

4.2.3 Results and discussion

4.2.3.1 Co-localization of siRNA in endosome/lysosome

We investigated the endosomal escape by subcellular distribution using CLSM image with 1 h and 8 h treatment of LNPs at pH 6.5 (Fig. 4.2).

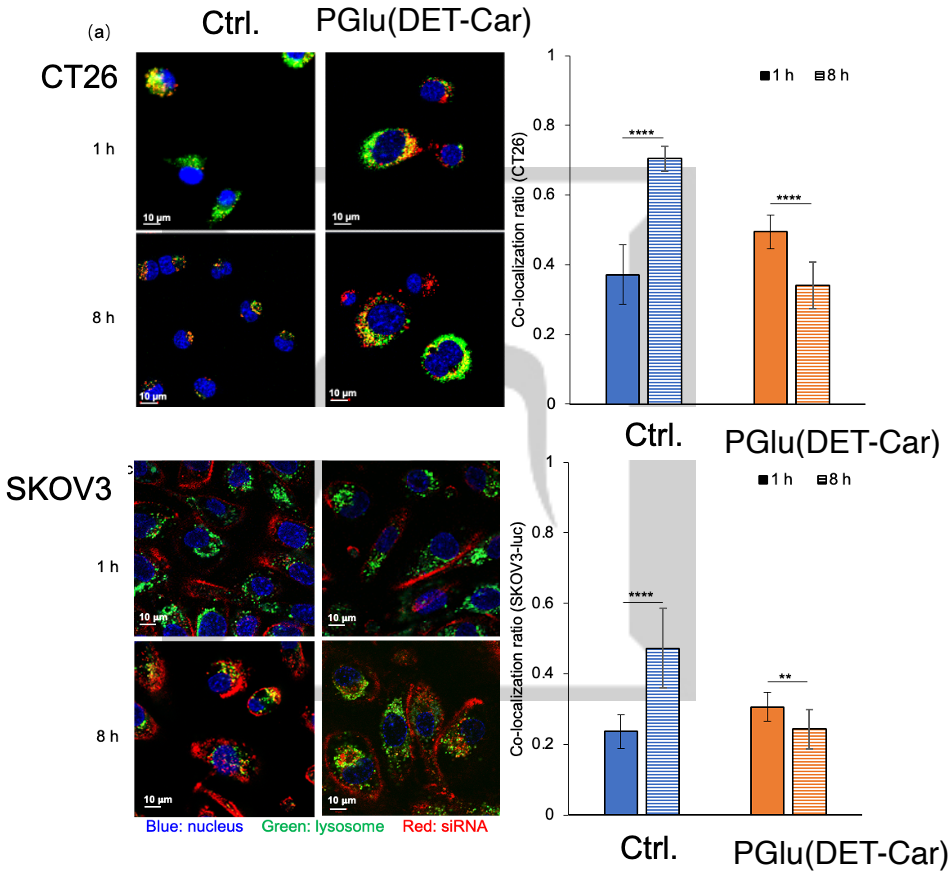

Figure 4.2 Assessment of endosomal escape. (a) CLSM image and (b) co-localization ratio of Alexa647-siGL3 and lyso/endosome in CT26 and SKOV3-luc. The cells were co-incubated with Alexa647-siGL3 loaded LNP for 1 h or 8 h at pH 6.5. Green, blue and red represent Lyso Tracker Red stained organelles, Hoechst 33342 stained nuclei and Alexa647-labeled siRNA. The results are shown as the mean ± S.D. (CT26: $n = 23$, SKOV3-luc: $n = 17$) Each result is expressed as the mean ± S.D., and ** $p<0.01$, **** $p<0.0001$ was considered significant.

Blue color is the nuclei, green color represents endosome/lysosome and red color shows Alexa-647. Yellow color exhibits the colocalization of Alexa-647-siRNA in endosome/lysosome as described in chapter 4.2.1.

In 1 h incubation, PGlu(DET-CAR)$_{30}$ LNP showed greater co-localization ratio of Alexa647-siRNA with Lyso Tracker Red stained organelles than control LNP (Fig. 4.2 b) in both CT26 and SKOV3-luc indicating that the rapid endocytosis of acidic pH-responsive PGlu(DET-CAR)$_{30}$ LNP compared to control LNP. After 8 h, co-localization ratio of PGlu(DET-CAR)$_{30}$ LNP significantly decreased and control LNP significantly increased regardless of cell line (Fig. 4.2 b) suggesting that PGlu(DET-CAR)$_{30}$ LNP led to efficient release of siRNA from endosome compared to control LNP.

4.2.3.2 Calcein release assay

To double check endosomal escape, siRNA-encapsulated LNPs were co-incubated with calcein for 1.5 h. As shown in Fig. 4.3, control LNPs showed punctuate calcein fluorescence demonstrated that calcein remained trapped inside endosomes. By contrast, PGlu(DET-CAR)$_{30}$ LNPs at pH 6.5 exhibited distinct diffusion of calcein to cytosol, which was observed in both CT26 and SKOV3-luc cells, indicating the successful endosomal escape. Together with

co-localization results, the internalized cationic LNPs caused by acidic pH-responsive PGlu(DET-Car) might efficiently induce endosomal escape through enhanced electrostatic interaction between the cationic LNP surface and the anionic endosomal membrane because of more acidic endosomal environment [66], as the ζ-potential measurement indicated an appreciable positive charge of PGlu(DET-CAR)$_{30}$ LNPs in acidic environment (Fig. 3.7), while ζ-potential of control LNPs remained almost neutral.

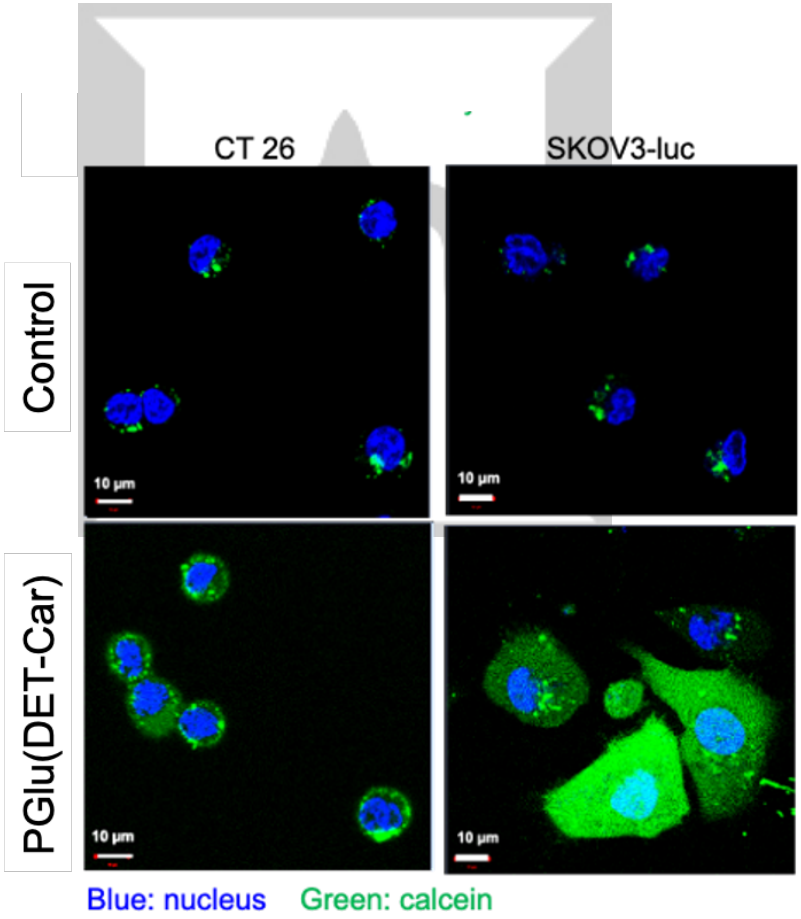

Figure 4.3 Cytosolic localization of calcein in SKOV3-luc and CT 26. The cells were incubated at pH 6.5 with the respective LNP solutions (100 nM of Alexa647-siGL3) for 1.5 h at 37 °C. The pictures show calcein (green), and nuclei stained by Hoechst 33342 (blue). Scale bar (white) = 10 µm.

Taken together, these results corroborate the more efficient endosomal escape capacity possessed by pH-responsive PGlu(DET-CAR)$_{30}$ LNPs compared to control LNPs.

4.3 Cytotoxicity

4.3.1 Introduction

In general, 24-96 h is the ideal periods for accessing siRNA knockdown in cell culture [73]. However, incubation in acidic media or treatment with highly positively charged particle might cause cytotoxicity. Therefore, we examined the cytotoxicity of LNPs for 24 h. We checked the cell viability among non-treatment (NT), PGlu(DET-CAR)$_{30}$ LNP and control LNP groups.

4.3.2 Materials and methods

SKOV3-luc cells were seeded in 96-well plates at a density of 2,500 cells/well with DMEM containing 10% FBS and 1% penicillin. After a 24 h incubation, cells were treated with fresh media (pH 6.5 or 7.4) containing siGL3-encapsulated LNPs at a final concentration of 100 nM siGL3. After 24 h incubation, a cell viability assay was performed using Cell Counting Kit-8. Absorbance at 450 nm was detected with a microplate absorbance reader. Cell viability was determined by the following equation:

Cell viability (%) = ([A]test – [A]blank)/([A]control – [A]blank) × 100%,

where *[A]test*, *[A]control*, and *[A]blank* are the absorbance values of the wells belonging to treated cells, non-treated cells (pH 7.4), and empty media, respectively.

4.3.3 Results and discussion

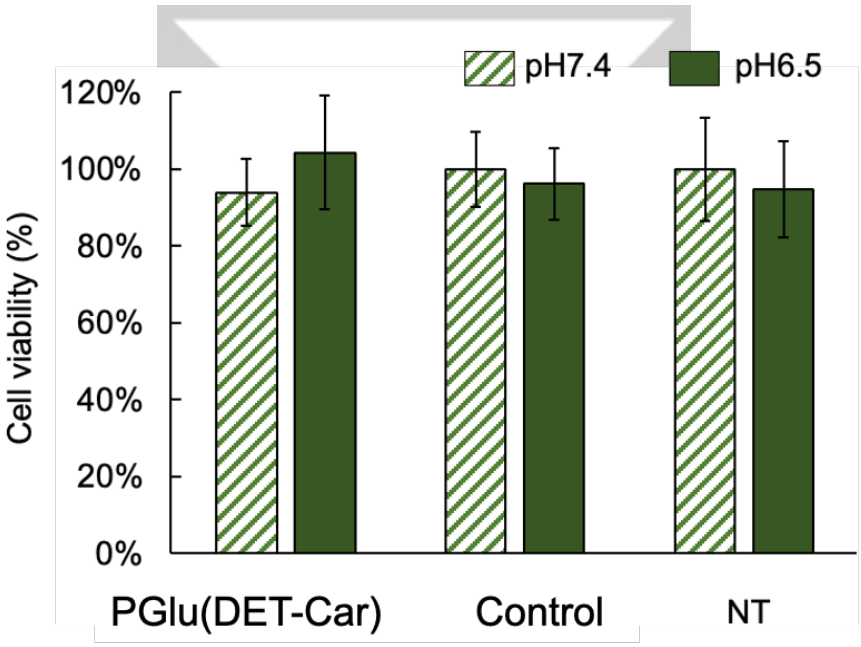

Figure 4.4. Cytotoxicity evaluation. Cell viability post-24 h within siGL3-encapsulated PGlu(DET-CAR)$_{30}$ LNPs, siGL3- encapsulated control LNPs, and non-treatment groups in SKOV3-luc at 100 nM dose siRNA at pH 7.4 and pH 6.5 (n=6).

As Fig. 4.4 showed, all groups had >90% cell viability in post-24 h treatment. In addition, there was no big difference of cell viability among

PGlu(DET-CAR)$_{30}$ LNP, control LNP and NT suggesting that the cytotoxicity from acidic pH and positively charged PGlu(DET-CAR)$_{30}$ LNP could be ignored.

4.4 *In vitro* gene silencing

4.3.1 Introduction

We had already confirmed successful cellular uptake and endosomal escape of LNPs and further confirmed the pH-responsive ability of PGlu(DET-CAR)$_{30}$ LNP having efficient cellular uptake and endosomal escape owing to the facilitated membrane-membrane interaction between cationic LNP and anionic plasma membrane (Fig. 4.1-4.3). As described in chapter 1.1.1, siRNA targets to mRNA and induces mRNA degradation which results in knockdown of gene expression.

Therefore, we examined the gene silencing activity of PGlu(DET-CAR)$_{30}$ LNP in this chapter. Here, we used SKOV3-luc cells which express the firefly luciferase gene and siGL3-encapsulated PGlu(DET-CAR)$_{30}$ LNP to knockdown the luciferase activity. This method is known as luciferase reporter assay which is used to determine whether a protein of interest regulates a particular gene at the transcription level [74, 75]. According to the knockdown the activity of luciferase compared to NT and control LNP, we could understand the gene

silencing activity of PGlu(DET-CAR)$_{30}$ LNP.

4.3.2 Materials and methods

SKOV3-luc cells were seeded in 24-well plate (5×10^4 cells/well) in DMEM containing 10% FBS and 1% penicillin followed by a 24 h incubation. After washing twice with PBS, the cells were treated with pH 6.5 media containing siGL3-loaded LNPs at a final concentration of 100 nM siRNA. After a 6 h incubation, subsequently, the media was replaced by fresh DMEM containing 10% FBS and 1 % penicillin, and the cells were allowed to incubate for a further 24 h. Following media removal and washing with PBS, cells were lysed by Passive Lysis Buffer for 30 min incubation, after which the supernatant was transferred to 96-well white plates, and finally subjected to treatment with luciferin. A microplate luminometer was used to measure relative luminescence units (RUL) of cells. Gene silencing efficiency was calculated based on the reduction in RLU compared with non-treatment (NT) cells.

The values are expressed as the mean ± standard deviation (SD). Statistical analysis was conducted using one-way ANOVA with Tukey's multiple comparisons test. A p value of < 0.05 was considered statistically significant.

4.3.3 Results and discussion

In vitro gene silencing activity of siGL3-encapsulated PGlu(DET-CAR)$_{30}$ LNPs was investigated in SKOV3-luc cells using a luciferase assay as Fig. 4.5 showed. In spite of the fact that both PDGC LNPs and the control LNPs exhibited the gene silencing, the PGlu(DET-CAR)$_{30}$ LNPs showed a significantly enhanced reduction due to the charge-switchable property. This result is in good agreement with the facilitated cellular uptake and endosomal escape as demonstrated in Fig. 4.1-4.3.

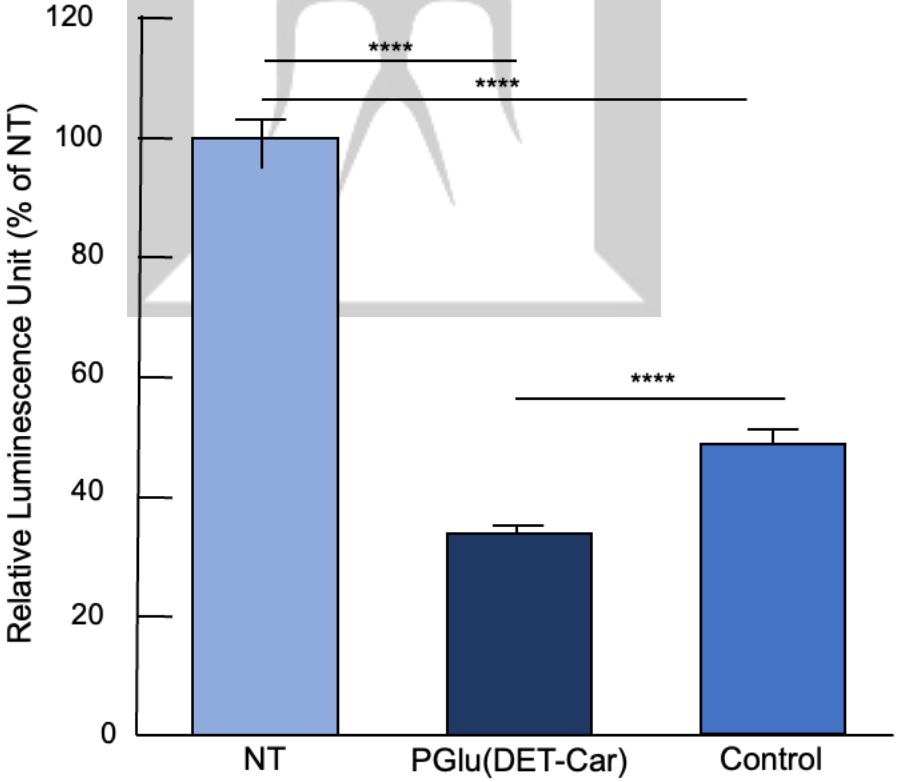

Figure 4.5 *In vitro* gene silencing efficiency of LNPs by luciferase assay. SKOV3-luc cells were treated with siGL3-encapsulated PGlu(DET-Car)$_{30}$ LNP and non-pH-responsive control LNP at pH 6.5 for 6 h followed by

incubation in fresh media for another 24 h. The siRNA dose was 100 nM. The results are shown as the mean ± S.D. (n = 7), **** $p < 0.0001$ (Tukey's multiple comparisons test).

The pH-dependent protonation of the amino groups of DET-Car within the endosomal lumen may result in osmotic swelling and subsequent endosome disruption *via* proton sponge effect [76]. As Fig. 4.6 showed, proton sponge effect results in lysosomal swelling and rupture, with materials released into the cytosol [77].

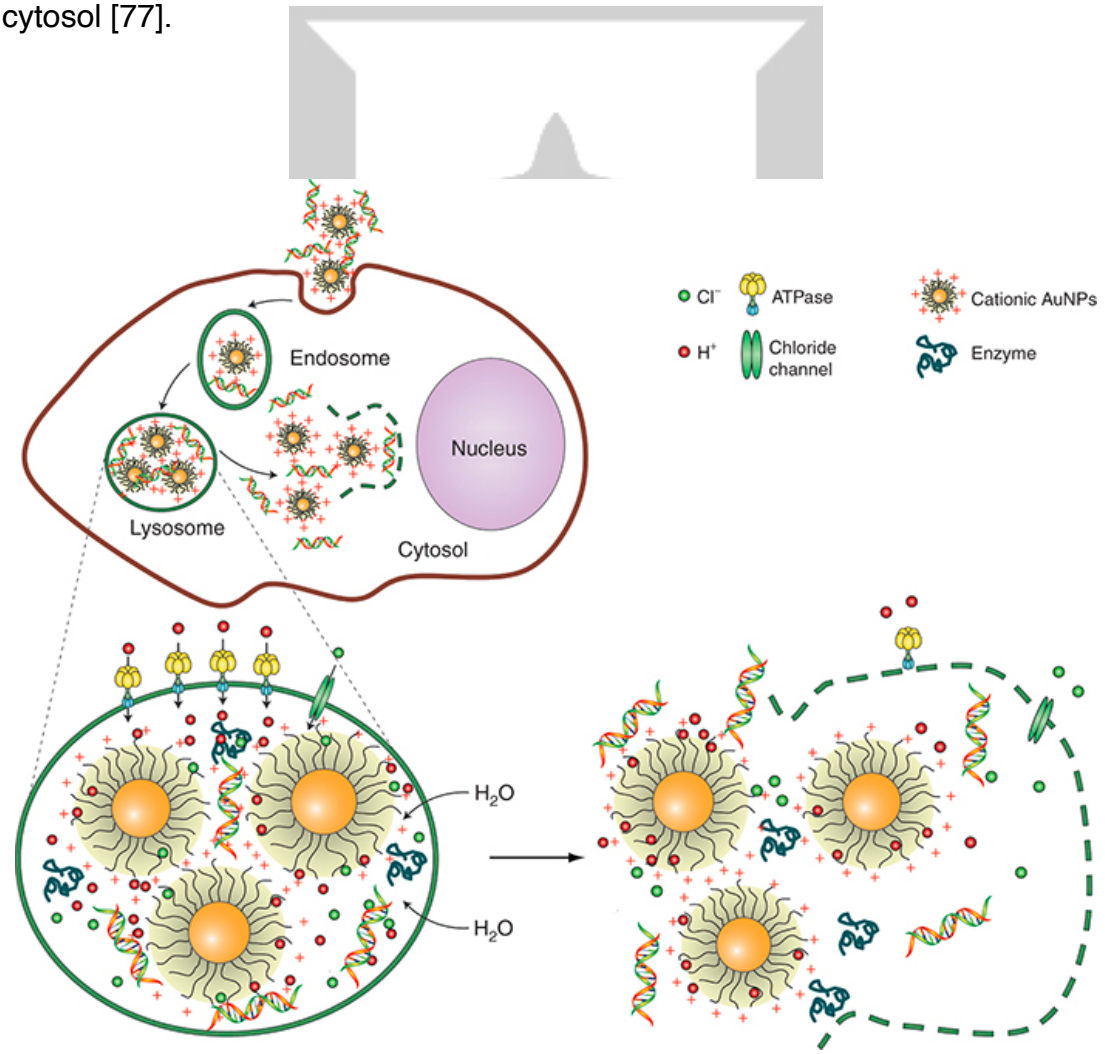

Figure 4.6. Schematic illustration of the proton sponge effect leading to endosomal escape for cationic nanoparticles [77].

Thus, the ionizable PGlu(DET-Car)$_{30}$ LNP achieved more efficient gene knockdown in cells compared with control LNP. As a consequence, the higher *in vitro* gene knockdown was found for acidic pH-responsive PGlu(DET-CAR)$_{30}$ LNPs in comparison with control LNPs (Fig.4.5).

Chapter 5 *In vivo* assessment

5.1 Biodistribution

5.1.1 Introduction

In last chapter, we confirmed the efficient cellular uptake, endosomal escape as well as gene silencing activity of cancerous pH-responsive PGlu(DET-CAR)$_{30}$ LNP over non-pH-responsive control LNP, which resulted from charge switchable nature of polyzwitterion modified onto LNP surface. In the *in vitro* assessment, we mimicked the cancerous environments through adjusting the pH of culture media. In this chapter, we examined the differences of *in vivo* behavior of PGlu(DET-CAR)$_{30}$ LNP in comparison with control LNP.

Once LNP has entered the vascular system, it is distributed throughout the body fluids according to the physiochemical properties of the LNP and its ability

to penetrate the barriers as describe in chapter 1.2. Therefore, we evaluate the biodistribution which means the transfer of LNPs after intravenous (i.v.) administration.

In biodistribution study, we checked the fluoresce intensity of Alexa647-labeled siRNA distributed in blood, tumor, liver, spleen, kidney, lung and heart. Note, the fluorescence of Alexa647-siRNA encapsulated inside LNP was too week to detect (Data were not showed). Nevertheless, detergent was necessary to destroy the LNP membrane to release the siRNA. Here, we used sodium dodecyl sulfate (SDS) dissolved in t-BuOH aqueous solution as demulsification agent. Li et. al., reported similar methods of demulsification agent used in biodistribution study of liposome [78].

5.1.2 Materials and methods

BALB/c (female, 4 weeks old) were obtained from Charles River Laboratories Japan Inc. All animal experiments were approved by the Animal Care and Use Committee and performed in accordance with the Guidelines for the Care and Use of Laboratory Animals set forth by Tokyo Institute of Technology.

A subcutaneous CT26 bearing model was built through subcutaneously

inoculating CT26 cells (5×10^5 cells per mouse) into BALB/c mice. When the tumor size reached approximately 200 mm^3, Alexa-647-labeled siGL3-loaded PGlu(DET-CAR)$_{30}$ LNPs and control LNPs were intravenously (i.v.) injected into mice (siRNA dose: 0.5 mg/kg). After 1 h, 6 h, and 24 h post-administration, blood was obtained from the inferior vena cava and then was heparinized. The tumors and other organs were collected and subsequently homogenized in lysis buffer, followed by centrifugation. The mice were then euthanized. Blood was collected and subsequently homogenized in lysis buffer, followed by centrifugation. After demulsification through mixing of supernatant with 3% SDS in 60% *t*-BuOH solution, the fluorescence intensity of Alexa-647-labeled siRNA in the plasma was measured by a microplate reader (Ex: 630 nm, Em: 690nm). The tumor accumulation of Alexa-647-labeled siGL3-loaded PGlu(DET-CAR)$_{30}$ LNPs and control LNPs was also studied with subcutaneous SKOV3-luc tumor models that were prepared by subcutaneous inoculation of SKOV3-luc cells (5×10^6 cells per mouse) into BALB/c nude mice. When the tumor size reached approximately 200 mm^3, PGlu(DET-CAR)$_{30}$ LNPs and control LNPs were intravenously injected and the tumor accumulation of siRNA at 6 and 24 h post-administration was evaluated in a similar manner as described above.

The values are expressed as the mean ± standard error of mean (SEM).

Statistical analysis was conducted using two-way ANOVA with Sidak's multiple comparisons test. A p value of < 0.05 was considered statistically significant.

5.1.3 Results and discussion

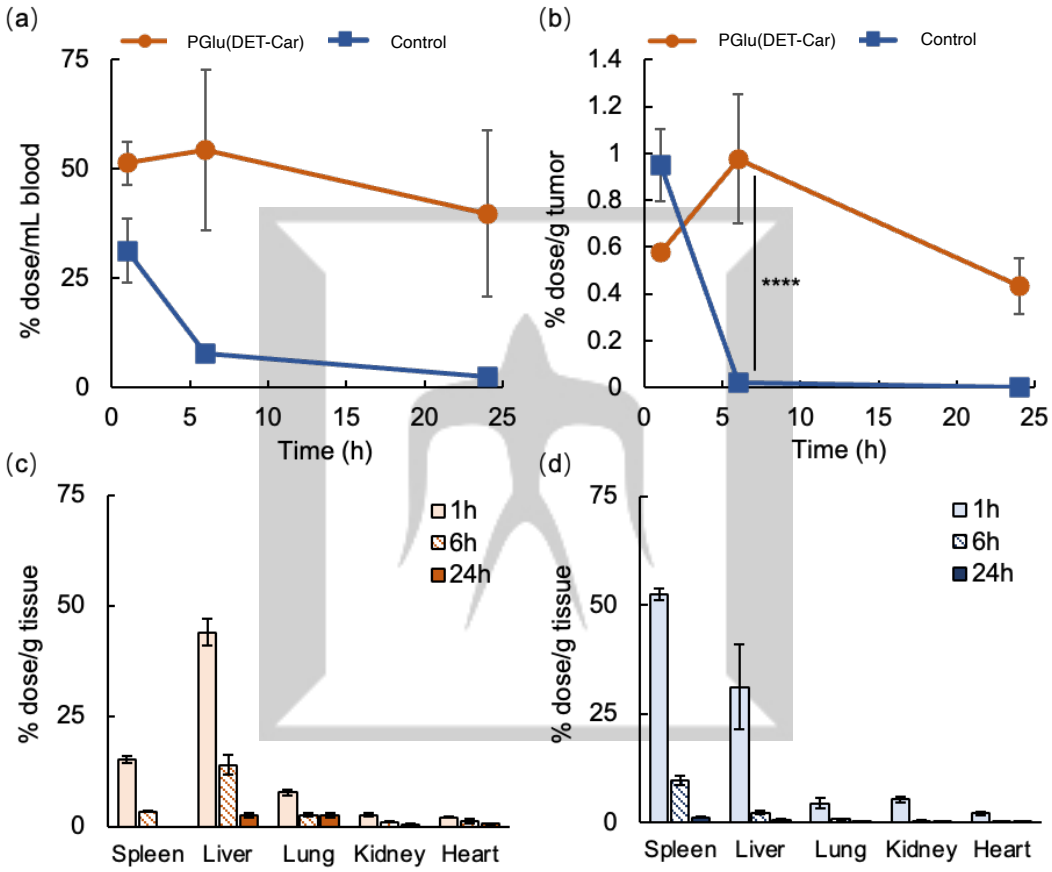

Figure 5.1 Biodistribution in CT26 subcutaneous models after i.v. administration of Alexa647-siGL3-loaded PGlu(DET-CAR)$_{30}$ and control LNPs (a) Blood circulation. (b) Tumor accumulation. Other organs accumulation of (c) PGlu(DET-CAR)$_{30}$ LNPs and (d) control LNPs. (n=3, two-way ANOVA with Sidak's multiple comparisons test). Each result is expressed as the mean ± SEM, and ****p<0.0001 was considered significant.

The *in vivo* biodistribution of Alexa647-siGL3-encapsulated PGlu(DET-

CAR)$_{30}$ LNP and PEGylated control LNP was assessed using a CT26 tumor-bearing mouse model as Fig. 5.1 showed.

Cancerous pH-responsive PGlu(DET-CAR)$_{30}$ LNP exhibited prolonged blood circulation and significantly higher tumor accumulation compared with control LNP (Fig. 5.1 a-b). It is worth mentioning that PGlu(DET-CAR)$_{30}$ LNP was able to maintain the greatly higher tumor retention level after 24 h while control LNP showed a sharp decline 6 h later. Meanwhile, both PGlu(DET-CAR)$_{30}$ LNP and control LNP demonstrated considerable accumulation within liver and spleen as Fig. 5.1 c-d showed, suggesting that their mechanism of clearance may be mediated by the MPS as described in chapter 1.2. However, PGlu(DET-Car)$_{30}$ modified LNP showed an apparently lower retention n in spleen than PEG modified LNP (Fig. 5.1 c-d). Although the mechanism of relatively low splenic accumulation of PGlu(DET-CAR)$_{30}$ LNP is still under investigation, the surface modification of PGlu(DET-Car)$_{30}$ onto LNP might cause distinct accumulation behavior in spleen probably due to the stealth ability difference of surface material. Thus, the sustained tumor accumulation behavior of PGlu(DET-CAR)$_{30}$ LNP is assumed to be due to the cationic charge of PGlu(DET-CAR)$_{30}$ LNP within cancerous pH as well as prolonged blood circulation.

PGlu(DET-CAR)$_{30}$ LNP showed prolonged blood circulation (Fig. 5.1 a), as polycarboxybetaine-coated liposomes demonstrated the longevity in the blood circulation [79]. As discussed in chapter 3.2.3.1, the anti-fouling property of polyzwitterions attributes to their formation of hydration layers with water molecules based in ion-dipole interactions [80, 81]. The polyzwitterion structure of PGlu(DET-Car)$_{30}$ might influence the affinity to serum proteins in bloodstream, in which further understanding the relationship between the physicochemical characteristics of PGlu(DET-CAR)$_{30}$ LNPs and their *in vivo* behavior will be required.

Once PGlu(DET-CAR)$_{30}$ LNP was protonated in response to acidic pH, the strong electrostatic interaction of PGlu(DET-CAR)$_{30}$ LNP with the negatively charged cell membranes of the cancer cells led to the extended intratumoral retention. Such a process is not readily available to non-pH-responsive control LNP, which consequently experience only a transient sojourn in cancer tissue.

5.2 In vivo gene silencing

5.2.1 Introduction

In vitro gene silencing (chapter 4.3) together with tumor accumulation (chapter 5.1) results indicate the *in vivo* availability of PGlu(DET-Car) modified

LNP in nucleic acid delivery. In this chapter, we examined the *in vivo* gene silencing activity of this novel siRNA carrier PGlu(DET-CAR)$_{30}$ LNP. We applied luciferases activity and reverse transcription polymerase chain reaction (RT-PCR) to evaluate the *in vivo* knockdown ability of LNPs *via* protein and mRNA level.

In bioluminescence approach, the whole animal bioluminescence imaging can be observed by *in vivo* imaging system (IVIS) with the intraperitoneal (i.p.) injection of luciferin. We compared the reduction level of luminous intensity between 24 h and 0 h after 24 h post-i.v. injection of siGL3-encapsulated LNPs.

Polymerase chain reaction (PCR) is a widely used method to rapidly amplifier a very small sample of DNA. For mRNA detection, reverse transcription (RT) of RNA into DNA is necessary. The technique combining reverse transcription with PCR called RT-PCR.

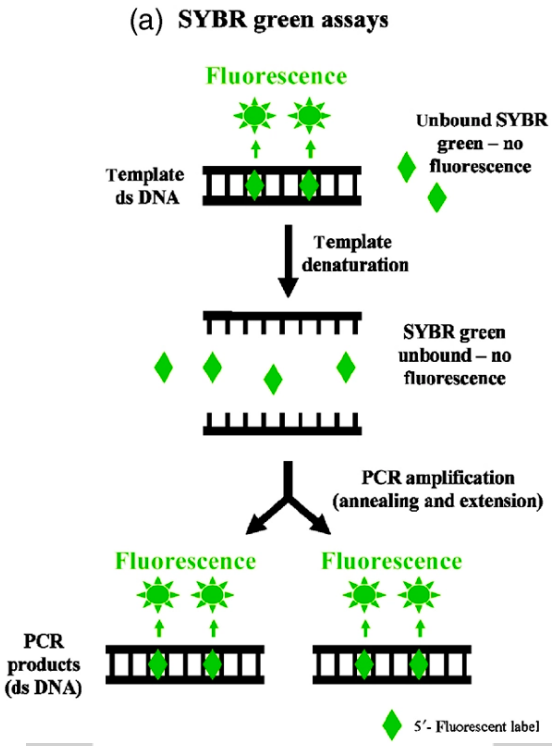

Figure 5.2 Mechanism of SYBR green used in PCR. SYBR green binds to all double-stranded DNA and emits a fluorescent signal. In its unbound state, SYBR green does not fluoresce [82].

SYBR green was applied to quantify the amplification level of mRNA in RT-PCR. As Fig. 5.2 showed, SYBR green binds to double-stranded DNA instead of single-stranded nucleic acids. Monitoring the amplification reaction using fluorescence is called real-time PCR or quantitative PCR. In qPCR, cycle of threshold (Ct) represents the amplification cycle of threshold, which is now commonly used in SARS-CoV-2 viral load determination [83]. Briefly, The Ct value increases with a decreasing amount of template, that is decreasing amount of target mRNA. Since Ct is a relative measure of the concentration of target template, control group (NT) is necessary to compare the Ct value of

sample and control. In order to make sure same volume of i.v. administration in each sample, NT group was i.v. injected D-PBS(-).

5.2.2 Materials and methods

5.2.2.1 *In vivo* gene knockdown *via* bioluminescence

Subcutaneous SKOV3-luc bearing mice (100 mm^3 of tumor size) were received i.p. injection of 6 mg VivoGloTM Luciferin and imaged by IVIS as 0 h time point. Then mice were i.v. injected siGL3-loaded LNPs at siRNA dose of 0.6 mg/kg or D-PBS(-) followed by i.p. injected same dose of luciferin and imaged by IVIS as 24 h time point. Gene knockdown as determined as inhibition of radiant efficiency of each group in 24 h compared to radiant efficiency in 0 h. Radiant efficiency measurement of the tumor luminescence was automatically assigned by the Live Image software used for image processing.

5.2.2.2 *In vivo* gene silencing *via* RT-PCR

Subcutaneous SKOV3-luc bearing mice (100 mm^3 of tumor size) were received i.v. injection of siGL3-loaded LNPs at siRNA dose of 0.5 mg/kg or PBS. After 24 h, 30 mg of tumor tissue was homogenized and RNA was isolated

using a RNeasy Protect Mini Kit according to the manufacturer's instructions. DNase I was used to remove DNA contamination followed by reverse transcription (RT) of the total RNA (5 μg for each sample) with PrimeScript RT reagent Kit with an oligo-dT primer. PCR were performed by PIKOREAL 96 Real-Time PCR System. The reaction mixtures contained 2 μg of cDNA with appropriate primer pairs and FastStart Universal SYBR Green Master. GL3 levels were calculated by the comparative Ct method using GAPDH as endogenous housekeeping genes. The value for non-treated cells was set to 1. The following primer pairs were used: GL3: 5′-TGAGTACTTCGAAATGTCCGTTC-3′ (forward); 5′-GTATTCAGCCCATATCGTTTCAT-3′ (reverse); GAPDH: 5′ -CCTCTGACTTCAACAGCGAC-3′ (forward); 5′ -GCCACATACCAGGAAATGAG-3′ (reverse).

5.2.3 Results and discussion

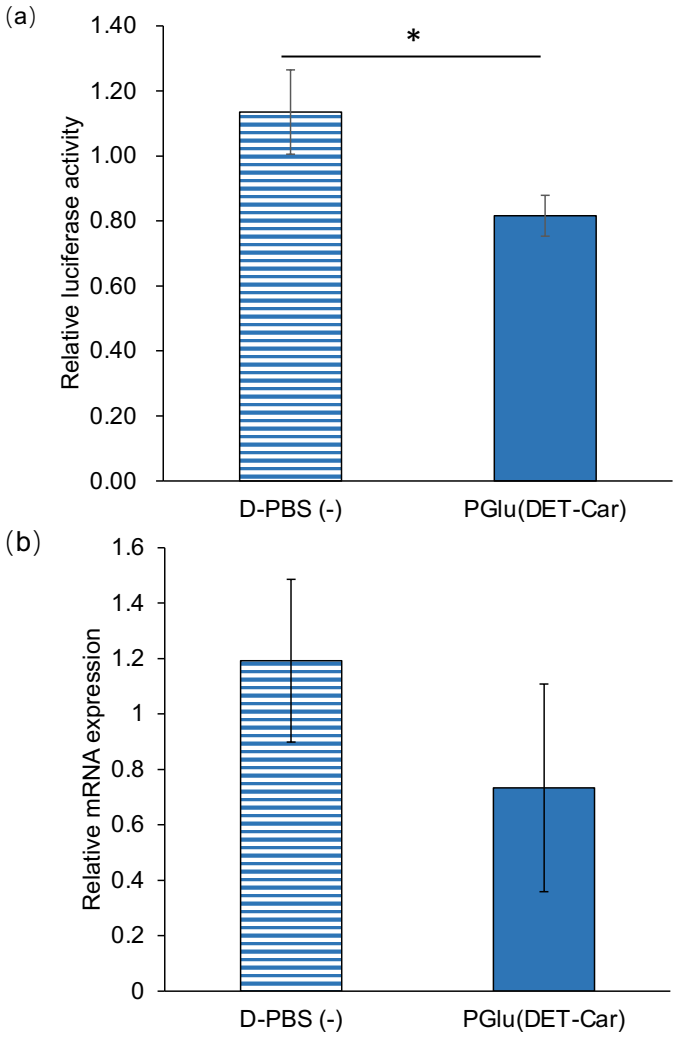

Figure 5.3 *In vivo* gene silencing assessment of PGlu(DET-CAR)$_{30}$ LNP. Gene knockdown ability was examined by (a) bioluminescent (n = 5) and (b) RT-PCR (n = 3) after 24 h post-i.v. injection of siGL3-encapsulated PGlu(DET-Car)$_{30}$ LNP and D-PBS(-). Each result is expressed as the mean ± S.E.M., * $p < 0.05$ (Student's *t*-test).

As Fig. 5.3 showed, the reduction of luciferase activity and mRNA expression suggested the *in vivo* gene silencing ability of PGlu(DET-CAR)$_{30}$ LNP *via* both bioluminescence and RT-PCR approaches in comparison with D-PBS(-) group. As Fig. 5.3 a showed, 24 h post-i.v. injection of siGL3-encapsulated PGlu(DET-CAR)$_{30}$ LNP led to the decreased radiant efficiency.

On the other hand, the slightly increased radiant efficiency of D-PBS(-) group (Fig. 5.3 a) possibly resulted from rapidly abnormal growth of cancer cells. Fig. 5.3 b shows the reduction of relative mRNA expression after 24 h post-i.v. injection of siGL3-encapsulated PGlu(DET-CAR)$_{30}$ LNP. Note, the average relative mRNA expression of D-PBS(-) group (slightly more than 1) (Fig. 5.3 b) was associated with calculation of comparative Ct method ($2^{-\Delta\Delta Ct}$ method). The Ct value of siGL3 and GAPDH of D-PBS(-) group was very close. The ΔCt of D-PBS(-) group calculated from the Ct difference between siGL3 and GAPDH was very slightly negative.

As described in chapter 1, siRNA carrier needs to pass through layers of barriers before it finally reaches cytosol. As Fig. 5.1 showed, the tumor accumulation of PGlu(DET-CAR)$_{30}$ LNP was about 1%. Besides, it is estimated that less than 2% of the siRNA administered *via* LNPs reaches the cytosol [69, 70]. Although it was difficult to estimate the anti-tumor effect of PGlu(DET-CAR)$_{30}$ LNP through *in vivo* gene silencing results which was one-time administration (Fig. 5.3), the *in vivo* knockdown ability in both mRNA and protein level together with biodistribution results (Fig. 5.1) indicated the potential of PGlu(DET-CAR)$_{30}$ LNP in nucleic acid delivery.

5.3 Anti-tumor effect

5.3.1 Introduction

In previous chapter, we confirmed the *in vivo* gene knockdown ability as described in chapter 5.2 *via* reduction of luciferase activity and mRNA expression compared to D-PBS(-) treatment (Fig. 5.2). After certifying the tumor accumulation and *in vivo* gene silencing activity of PGlu(DET-CAR)$_{30}$ LNP, the anti-tumor effect was examined using siPLK1-encapsulated LNPs in SKOV3-luc tumor-bearing mice. siPLK1 has been shown to interfere with mitosis and suppress proliferation of human cancer cells [84] The suppression of tumor growth can be evaluated through periodic i.v. administration of siPLK1-encapsulated PGlu(DET-CAR)$_{30}$ LNP.

5.3.2 Materials and methods

Anti-tumor study was evaluated using a SKOV3-luc tumor-bearing model, prepared as described above. When tumors reached 25 mm^3, mice were i.v. injected siPLK1-encapsulated PGlu(DET-CAR)$_{30}$ LNP and control LNP (siRNA dose: 2.5 mg/kg) every other day. The tumor volume (V) was calculated using the following equation.

$$V\ (mm^3) = ab^2/2,$$

where *a* and *b* are the major and minor axes of the tumor, respectively. Mice were euthanized upon tumor growth to 200 mm^3.

The values are expressed as the mean ± standard error of mean (SEM). Statistical analysis was conducted using two-way ANOVA with Tukey's multiple comparisons test. A p value of < 0.05 was considered statistically significant.

5.3.3 Results and discussion

siPLK1-encapsulated LNPs at a dose of 2.5 mg/kg siPLK1 were administrated through periodic i.v. injection as shown in Fig. 5.4 a. In comparison with both siPLK1-encapsulated control LNP and NT groups, siPLK1-encapsulated PGlu(DET-Car)$_{30}$ LNP significantly suppressed tumor growth without loss of the body weight (Fig. 5.4 b-c). The pH-responsive property and slower clearance of PGlu(DET-Car)$_{30}$ LNP (Fig. 5.1) led to enhanced tumor accumulation compared to control LNP, and therefore resulted in siRNA delivery at a level adequate for tumor growth suppression.

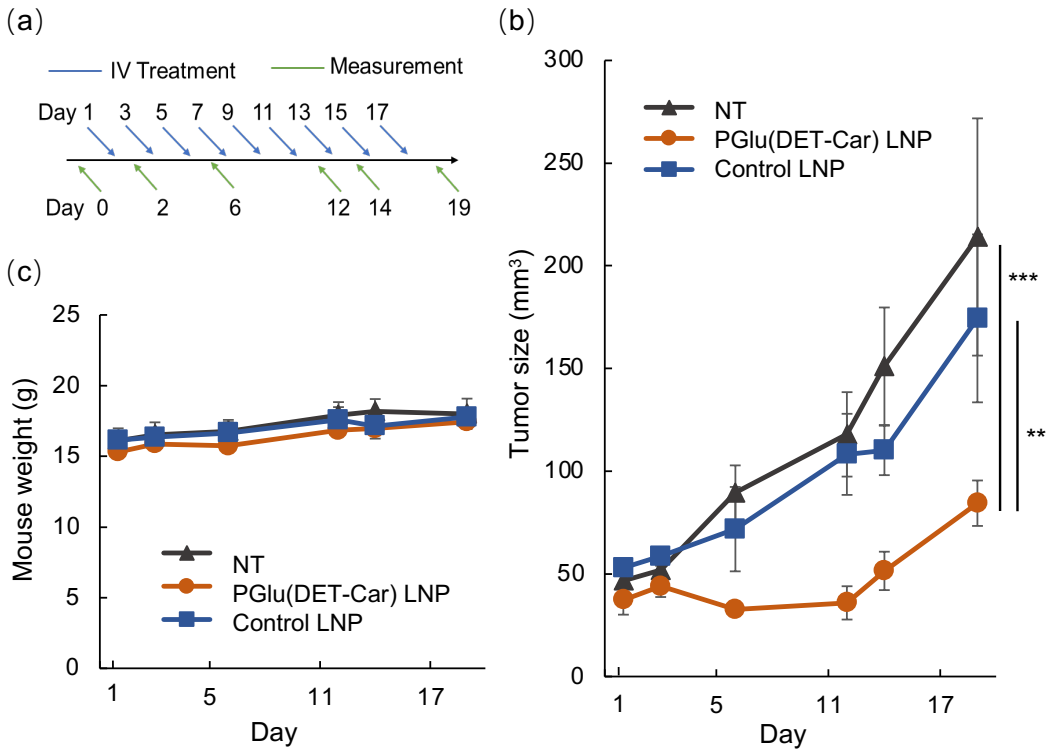

Figure 5.4 Anti-tumor effect. (a) Scheme of therapeutic regimen. (b) Tumor suppression effect and (v) mouse body weight change during periodic i.v. administration of siPLK1-loaded LNPs. Each point is expressed as the mean ± S.E.M. (n = 4), ** $p < 0.01$, and *** $p < 0.001$ (two-way ANOVA with Tukey's multiple comparisons test).

Despite the fact that tumor suppression efficacy lasted less than 2 weeks possibly due to the rapid growth nature of tumor cells (Fig. 5.4 b), tumor suppression effect of PGlu(DET-Car)$_{30}$ LNP was promising in comparison with control LNP. Moreover, PEGylated nanoparticles have been reported to be rapidly removed from circulation upon administration of subsequent doses [85]. Although we did not investigate whether repeated injection of PGlu(DET-Car)$_{30}$ LNP would cause quick blood clearance, PGlu(DET-Car)$_{30}$ LNP significantly improved tumor growth suppression over control LNP. As described in chapter

5.1, anti-fouling property of polyzwitterion further enhanced the anti-tumor effect of PGlu(DET-Car)$_{30}$ LNP.

Considering the tumor accumulation as Fig. 5.1 a showed, half-life of PGlu(DET-Car) LNP was estimated to be 24 h. Administration of 2.5 mg/kg every other day (Fig. 5.4 a and c) seemed to be insufficient for SKOV3-luc model. However, current limitation of this system is that siRNA-encapsulated LNP prepared by alcohol dilution method could not scale-up. Microfluidic device such as NanoAssemblr™ might be a good platform to scale-up the LNP preparation.

In summary, we demonstrated that PGlu(DET-Car) modified LNP showed cancerous pH-responsive enhancement in cellular uptake, endosomal escape and gene silencing *in vitro* and enabled successful delivery of therapeutic siRNA in the subcutaneous tumor models. These results strongly signify the utility of PGlu(DET-Car) as a smart surface modification material for systemic delivery of siRNA payloads to malignant tumors.

Chapter 6 Conclusion & Future perspective

6.1 Conclusion

In current nucleic acid encapsulated LNP system, there is no suitable carrier that possess both tumor targeting and gene delivery ability. Although more and more ionizable lipids were developed to enhance gene transfer efficiency, PEGylation which is necessary for circulation limits the delivery to tumor, not to mention the fact that those ionizable lipids used in commercial drug are all under patent protection.

In this study, we successfully constructed a cancerous pH-responsive siRNA-encapsulated LNP system for effective tumor accumulation and nucleic acid delivery over PEGylated control LNP. siRNA-encapsulated PGlu(DET-CAR)$_{30}$ LNP expressed fine-tuned charge-responsive ability, high encapsulation efficiency as well as good serum stability. Moreover, PGlu(DET-CAR)$_{30}$ LNP also showed superior cellular uptake and endosomal escape especially at cancerous pH (6.5) compared to control group. Importantly, PGlu(DET-CAR)$_{30}$ LNP revealed successful gene silencing both *in vitro* and *in vivo*. Neutrality in physiological, cationic charge in tumor acidic microenvironment as well as anti-biofouling property of PGlu(DET-Car)

contributed to high tumor accumulation and extended blood circulation.

Most important of all, owing to these advantages, periodic i.v. administration of siPLK1-encapsulated LNP successfully inhibited tumor growth in comparison to control LNP. These results demonstrate that this smart pH-responsive polyzwitterion-modified LNP system is an excellent candidate to be a novel biomaterial for gene cancer therapy.

6.2 Future perspective

We demonstrated that cancerous pH-responsive PGlu(DET-Car) modified LNP achieved better tumor accumulation, blood circulation and gene silencing than control LNP. However, there are still limitations existed in this system.

First of all, the tumor retention of PGlu(DET-CAR)$_{30}$ LNP (1 %) is still not high enough. Since zwitterion interacts with water molecular *via* ionic bond, and surface modification of zwitterionic polymer that forms hydration layer stabilize LNP structure and prevent protein adsorption. It is worthy to further optimizing this system through increasing polymer chain (degree of polymer > 30) to strengthen the stealth effect of hydration layer and membrane-membrane interaction between polyzwitterion and plasma membrane.

Secondly, clarifying the mechanism of low splenic accumulation and long

blood circulation of PGlu(DET-CAR)$_{30}$ LNP over PEGylated control group are meaningful to understand the *in vivo* behavior of PGlu(DET-Car) especially in the unique anti-fouling property. Besides, investigating the immune response of PGlu(DET-Car) surface modification is crucial for future clinical application.

Furthermore, scale-up the LNP preparation is essential for the whole LNP trials especially for *in vivo* assessments which needs much higher siRNA dose than *in vitro* assessments. Owing to the global demand for SARS-CoV-2. mRNA vaccine production, Pfizer/BioNTech and Moderna used a microfluidics-based production such as the NanoAssemblr® (Precision Nanosystems, Vancouver, BC, Canada) platforms [86]. In addition to the scale-up process, microfluidic device also helps to form smaller particle size and polydispersity due to the advantages of the use of strictly laminar flow, short molecular diffusion distances as well as low energy consumption [86]. Current siRNA-encapsulated PGlu(DET-Car) LNP system prepared by *t*-BuOH dilution is a diamond in the rough. Optimization through microfluidic device has great potentialities to yield more suitable LNP with small and uniform particle. It is excited to see the future application of PGlu(DET-Car) LNP in a wide variety of nucleic acid delivery.

Appendix

Reagent information

DCM, AcN, THF, HEPES, MES, sodium acetate, HCl and SDS were purchased from Wako Pure Chemical Industries, Ltd. (Osaka, Japan). DSPE-PEG_4-DBCO was purchased from BroadPharm (San Diego, CA, USA). Cholesterol, DOPE and DOTAP were purchased from AvantiPolar Lipids Inc. (Alabaster, AL, USA). DSPE-$PEG_{5k,}$ DSPE-PGlu(DET-Car)$_{30}$ was obtained from NOF Corporation (Tokyo, Japan). D-PBS(-) and *t*-BuOH were purchased from Nacalai Tesque Inc (Kyoto, Japan). RiboGreen® RNA reagent, LysoTracker Red DND-99 and Hoechst 33342 were purchased from Thermo Fisher Scientific (Waltham, MA, USA). siRNA against luciferase (siGL3, sense: 5′-CUUACGCUGAGUACUUCG AdTdT-3; antisense: 5′-UCGAAGUACUCAGCGUAAGdTdT-3′), Alexa647-labeled siRNA (Alexa647-siGL3, sense: 5′-CUUACGCUGAGUACUUCG AdTdT-3′; antisense: 5′-Alexa647-UCGAAGUACUCAGCGUAAGdTdT-3′), and siRNA against polo-like kinase-1 (siPLK1, sense: 5′-AGAUCACCCUCCUUAAAUAUU-3′; antisense: 5′-UAUUUAAGGAGGGUGAUCUUU-3′) were synthesized by GeneDesign, Inc. (Osaka, Japan). Calcein and Cell Counting Kit-8 was obtained from Dojindo,

Kumamoto, Japan. Passive Lysis Buffer and VivoGloTM Luciferin were purchased from Promega Corporation, Madison, WI, USA. RNeasy Protect Mini Kit was obtained from QIAGEN, Hilden, Germany. DNase I and PrimeScript RT reagent Kit were purchased from Takara Bio Inc. Shiga, Japan. Triton X-100, dextran sulfate, FBS, DMEM, penicillin, trypsin/EDTA, and SYBR Green Master was obtained from Merck Millipore, Burlington, MA, USA.

Cell lines and animals

SKOV3-luc were provided by the Japanese Collection of Research Bioresources (JCRB) Cell Bank through the National Institutes of Biomedical Innovation, Health and Nutrition (Osaka, Japan). CT26 were purchased from ATCC (Manassas, VA, USA). Cells were sub-cultured in DMEM with 10% FBS and 1% penicillin, and were maintained at 37 °C in an incubator (5% CO_2, 95% humidified environment). BALB/c and BALB/c nude mice (female, 4 weeks old) were obtained from Japan SLC Inc. (Hamamatsu, Japan). All animal experiments were approved by the Animal Care and Use Committee and performed in accordance with the Guidelines for the Care and Use of Laboratory Animals set forth by Tokyo Institute of Technology.

Equipment information

Nuclear Magnetic Resonance:

400 MHz NMR Spectrometer Bruker Biospin AG AVANCE III, Billerica, MA, USA.

High Performance Liquid Chromatography:

Jasco HPLC system equipped with UV detector (240 nm), Tokyo, Japan.

HPLC Column:

Inertsil WP300 C18 (4.6 × 250 mm) GL science

Zetasizer:

Zetasizer Nano-ZS90, Malvern, UK.

Transmission Electron microscopy:

JEM-1010BS, JEOL, Tokyo, Japan.

Microplate Reader:

SPARK TKS01, TECAN, Zürich, Switzerland.

Flow Cytometer:

Guava® easyCyte™, Malvern, UK.

Confocal Laser Scanning Microscope:

LSM710, Carl Zeiss AG, Oberkochen, Germany.

Microplate Absorbance Reader:

iMark™ Microplate Absorbance Reader, Bio-Rad Laboratories, Inc., Hercules, CA, USA.

Luminometer:

GloMax® 96 Microplate Luminometer, Promega Corporation, Madison, WI, USA.

***In Vivo* Imaging System:**

IVIS® Spectrum In Vivo Imaging System, Perkin Elmer, Waltham, MA, USA.

RT-PCR:

PIKOREAL 96 Real-Time PCR System, Thermo Scientific™, Waltham, MA, USA.

References

[1] G. Watts, Work on RNA interference brings Nobel triumph, Bmj 333(7571) (2006) 717.

[2] A.J. Hamilton, D.C. Baulcombe, A species of small antisense RNA in posttranscriptional gene silencing in plants, Science 286(5441) (1999) 950-2.

[3] S.M. Elbashir, J. Harborth, W. Lendeckel, A. Yalcin, K. Weber, T. Tuschl, Duplexes of 21-nucleotide RNAs mediate RNA interference in cultured mammalian cells, Nature 411(6836) (2001) 494-8.

[4] E. Bernstein, A.A. Caudy, S.M. Hammond, G.J. Hannon, Role for a bidentate ribonuclease in the initiation step of RNA interference, Nature 409(6818) (2001) 363-366.

[5] A.J. Pratt, I.J. MacRae, The RNA-induced silencing complex: a versatile gene-silencing machine, J Biol Chem 284(27) (2009) 17897-901.

[6] S. Mocellin, M. Provenzano, RNA interference: learning gene knock-down from cell physiology, Journal of Translational Medicine 2(1) (2004) 39.

[7] X. Chen, L.S. Mangala, C. Rodriguez-Aguayo, X. Kong, G. Lopez-Berestein, A.K. Sood, RNA interference-based therapy and its delivery systems, Cancer and Metastasis Reviews 37(1) (2018) 107-124.

[8] A. Wittrup, J. Lieberman, Knocking down disease: a progress report on

siRNA therapeutics, Nature Reviews Genetics 16(9) (2015) 543-552.

[9] S.R. Youngren-Ortiz, N.S. Gandhi, L. España-Serrano, M.B. Chougule, Aerosol Delivery of siRNA to the Lungs. Part 2: Nanocarrier-based Delivery Systems, Kona 34 (2017) 44-69.

[10] H. Song, S.L. Hart, Z. Du, Assembly strategy of liposome and polymer systems for siRNA delivery, International Journal of Pharmaceutics 592 (2021) 120033.

[11] A. Babu, R. Muralidharan, N. Amreddy, M. Mehta, A. Munshi, R. Ramesh, Nanoparticles for siRNA-Based Gene Silencing in Tumor Therapy, IEEE Trans Nanobioscience 15(8) (2016) 849-863.

[12] J.A. Kulkarni, D. Witzigmann, S. Chen, P.R. Cullis, R. van der Meel, Lipid Nanoparticle Technology for Clinical Translation of siRNA Therapeutics, Accounts of Chemical Research 52(9) (2019) 2435-2444.

[13] P. Ghasemiyeh, S. Mohammadi-Samani, Solid lipid nanoparticles and nanostructured lipid carriers as novel drug delivery systems: applications, advantages and disadvantages, Res Pharm Sci 13(4) (2018) 288-303.

[14] B. Hu, Y. Weng, X.H. Xia, X.J. Liang, Y. Huang, Clinical advances of siRNA therapeutics, J Gene Med 21(7) (2019) e3097.

[15] Y. Weng, H. Xiao, J. Zhang, X.J. Liang, Y. Huang, RNAi therapeutic and its

innovative biotechnological evolution, Biotechnol Adv 37(5) (2019) 801-825.

[16] A. Figueiras, C. Domingues, I. Jarak, A.I. Santos, A. Parra, A. Pais, C. Alvarez-Lorenzo, A. Concheiro, A. Kabanov, H. Cabral, F. Veiga, New Advances in Biomedical Application of Polymeric Micelles, Pharmaceutics 14(8) (2022).

[17] H.M. Patel, S.M. Moghimi, Serum-mediated recognition of liposomes by phagocytic cells of the reticuloendothelial system - The concept of tissue specificity, Adv Drug Deliv Rev 32(1-2) (1998) 45-60.

[18] E. Blanco, H. Shen, M. Ferrari, Principles of nanoparticle design for overcoming biological barriers to drug delivery, Nat Biotechnol 33(9) (2015) 941-51.

[19] A.E. Nel, L. Mädler, D. Velegol, T. Xia, E.M.V. Hoek, P. Somasundaran, F. Klaessig, V. Castranova, M. Thompson, Understanding biophysicochemical interactions at the nano–bio interface, Nature Materials 8(7) (2009) 543-557.

[20] S. Tenzer, D. Docter, J. Kuharev, A. Musyanovych, V. Fetz, R. Hecht, F. Schlenk, D. Fischer, K. Kiouptsi, C. Reinhardt, K. Landfester, H. Schild, M. Maskos, S.K. Knauer, R.H. Stauber, Rapid formation of plasma protein corona critically affects nanoparticle pathophysiology, Nature Nanotechnology 8(10) (2013) 772-781.

[21] H. Soo Choi, W. Liu, P. Misra, E. Tanaka, J.P. Zimmer, B. Itty Ipe, M.G. Bawendi, J.V. Frangioni, Renal clearance of quantum dots, Nature Biotechnology 25(10) (2007) 1165-1170.

[22] R.R. Arvizo, O.R. Miranda, D.F. Moyano, C.A. Walden, K. Giri, R. Bhattacharya, J.D. Robertson, V.M. Rotello, J.M. Reid, P. Mukherjee, Modulating pharmacokinetics, tumor uptake and biodistribution by engineered nanoparticles, PLoS One 6(9) (2011) e24374.

[23] J.M. Harris, R.B. Chess, Effect of pegylation on pharmaceuticals, Nature Reviews Drug Discovery 2(3) (2003) 214-221.

[24] H. Hatakeyama, H. Akita, H. Harashima, The Polyethyleneglycol Dilemma: Advantage and Disadvantage of PEGylation of Liposomes for Systemic Genes and Nucleic Acids Delivery to Tumors, Biological and Pharmaceutical Bulletin 36(6) (2013) 892-899.

[25] Y. Fang, J. Xue, S. Gao, A. Lu, D. Yang, H. Jiang, Y. He, K. Shi, Cleavable PEGylation: a strategy for overcoming the "PEG dilemma" in efficient drug delivery, Drug Deliv 24(sup1) (2017) 22-32.

[26] M.F. Attia, N. Anton, J. Wallyn, Z. Omran, T.F. Vandamme, An overview of active and passive targeting strategies to improve the nanocarriers efficiency to tumour sites, J Pharm Pharmacol 71(8) (2019) 1185-1198.

[27] F. Danhier, O. Feron, V. Préat, To exploit the tumor microenvironment: Passive and active tumor targeting of nanocarriers for anti-cancer drug delivery, Journal of Controlled Release 148(2) (2010) 135-146.

[28] H. Maeda, The 35th Anniversary of the Discovery of EPR Effect: A New Wave of Nanomedicines for Tumor-Targeted Drug Delivery-Personal Remarks and Future Prospects, J Pers Med 11(3) (2021).

[29] I. Negut, V. Grumezescu, Chapter 3 - Nanoparticles and hyperthermia, in: A.M. Grumezescu (Ed.), Biomedical Applications of Nanoparticles, William Andrew Publishing2019, pp. 63-90.

[30] L.C. Böckelmann, U. Schumacher, Targeting tumor interstitial fluid pressure: will it yield novel successful therapies for solid tumors?, Expert Opin Ther Targets 23(12) (2019) 1005-1014.

[31] S.N. Ekdawi, D.A. Jaffray, C. Allen, Nanomedicine and tumor heterogeneity: Concept and complex reality, Nano Today 11(4) (2016) 402-414.

[32] E. Huynh, G. Zheng, Cancer nanomedicine: addressing the dark side of the enhanced permeability and retention effect, Nanomedicine (Lond) 10(13) (2015) 1993-5.

[33] M.A. Subhan, S.S.K. Yalamarty, N. Filipczak, F. Parveen, V.P. Torchilin, Recent Advances in Tumor Targeting via EPR Effect for Cancer Treatment, J

Pers Med 11(6) (2021).

[34] K. Yokoi, T. Tanei, B. Godin, A.L. van de Ven, M. Hanibuchi, A. Matsunoki, J. Alexander, M. Ferrari, Serum biomarkers for personalization of nanotherapeutics-based therapy in different tumor and organ microenvironments, Cancer Lett 345(1) (2014) 48-55.

[35] X. Xie, Y. Zhang, F. Li, T. Lv, Z. Li, H. Chen, L. Jia, Y. Gao, Challenges and Opportunities from Basic Cancer Biology for Nanomedicine for Targeted Drug Delivery, Curr Cancer Drug Targets 19(4) (2019) 257-276.

[36] R.A. Gatenby, R.J. Gillies, Why do cancers have high aerobic glycolysis?, Nat Rev Cancer 4(11) (2004) 891-9.

[37] G. Helmlinger, F. Yuan, M. Dellian, R.K. Jain, Interstitial pH and pO2 gradients in solid tumors in vivo: high-resolution measurements reveal a lack of correlation, Nat Med 3(2) (1997) 177-82.

[38] Y. Kato, S. Ozawa, C. Miyamoto, Y. Maehata, A. Suzuki, T. Maeda, Y. Baba, Acidic extracellular microenvironment and cancer, Cancer Cell Int 13(1) (2013) 89.

[39] D. Neri, C.T. Supuran, Interfering with pH regulation in tumours as a therapeutic strategy, Nat Rev Drug Discov 10(10) (2011) 767-77.

[40] A. Som, S. Bloch, J.E. Ippolito, S. Achilefu, Acidic extracellular pH of

tumors induces octamer-binding transcription factor 4 expression in murine fibroblasts in vitro and in vivo, Sci Rep 6 (2016) 27803.

[41] M.V. Liberti, J.W. Locasale, The Warburg Effect: How Does it Benefit Cancer Cells?, Trends Biochem Sci 41(3) (2016) 211-218.

[42] A. Som, S. Bloch, J.E. Ippolito, S. Achilefu, Acidic extracellular pH of tumors induces octamer-binding transcription factor 4 expression in murine fibroblasts in vitro and in vivo, Scientific Reports 6(1) (2016) 27803.

[43] A.H. Ranneh, H. Takemoto, S. Sakuma, A. Awaad, T. Nomoto, Y. Mochida, M. Matsui, K. Tomoda, M. Naito, N. Nishiyama, An Ethylenediamine-based Switch to Render the Polyzwitterion Cationic at Tumorous pH for Effective Tumor Accumulation of Coated Nanomaterials, Angew Chem Int Ed Engl 57(18) (2018) 5057-5061.

[44] Z.-R. Lu, V.E.A. Laney, R. Hall, N. Ayat, Environment-Responsive Lipid/siRNA Nanoparticles for Cancer Therapy, Advanced Healthcare Materials 10(5) (2021) 2001294.

[45] P.R. Cullis, M.J. Hope, Lipid Nanoparticle Systems for Enabling Gene Therapies, Mol Ther 25(7) (2017) 1467-1475.

[46] M. Schlich, R. Palomba, G. Costabile, S. Mizrahy, M. Pannuzzo, D. Peer, P. Decuzzi, Cytosolic delivery of nucleic acids: The case of ionizable lipid

nanoparticles, Bioeng Transl Med 6(2) (2021) e10213.

[47] Y. He, Z. Mao, Y. Zhang, H. Lv, J. Yan, Y. Cao, R. Pei, Tumor Acid Microenvironment-Triggered Self-Assembly of ESIONPs for T1/T2 Switchable Magnetic Resonance Imaging, ACS Applied Bio Materials 3(11) (2020) 7752-7761.

[48] L. Shen, K. Cai, J. Yu, J. Cheng, Novel Liposomal Azido Mannosamine Lipids on Metabolic Cell Labeling and Imaging via Cu-Free Click Chemistry, Bioconjugate Chemistry 30(9) (2019) 2317-2322.

[49] W. Shi, F. Tang, J. Ao, Q. Yu, J. Liu, Y. Tang, B. Jiang, X. Ren, H. Huang, W. Yang, W. Huang, Manipulating the Click Reactivity of Dibenzoazacyclooctynes: From Azide Click Component to Caged Acylation Reagent by Silver Catalysis, Angew Chem Int Ed Engl 59(45) (2020) 19940-19944.

[50] C.T. Mant, Y. Chen, Z. Yan, T.V. Popa, J.M. Kovacs, J.B. Mills, B.P. Tripet, R.S. Hodges, HPLC analysis and purification of peptides, Methods Mol Biol 386 (2007) 3-55.

[51] X. Cheng, R.J. Lee, The role of helper lipids in lipid nanoparticles (LNPs) designed for oligonucleotide delivery, Advanced Drug Delivery Reviews 99 (2016) 129-137.

[52] P. Rockenfeller, M. Koska, F. Pietrocola, N. Minois, O. Knittelfelder, V. Sica, J. Franz, D. Carmona-Gutierrez, G. Kroemer, F. Madeo, Phosphatidylethanolamine positively regulates autophagy and longevity, Cell Death & Differentiation 22(3) (2015) 499-508.

[53] R.R. Meka, S. Godeshala, S. Marepally, K. Thorat, H.K. Reddy Rachamalla, A. Dhayani, A. Hiwale, R. Banerjee, A. Chaudhuri, P.K. Vemula, Asymmetric cationic lipid based non-viral vectors for an efficient nucleic acid delivery, RSC Advances 6(81) (2016) 77841-77848.

[54] J. Heyes, L. Palmer, K. Bremner, I. MacLachlan, Cationic lipid saturation influences intracellular delivery of encapsulated nucleic acids, J Control Release 107(2) (2005) 276-87.

[55] F. Köster, D. Finas, C. Schulz, C. Hauser, K. Diedrich, R. Felberbaum, Additive effect of steroids and cholesterol on the liposomal transfection of the breast cancer cell line T-47D, Int J Mol Med 14(4) (2004) 769-72.

[56] D.A. Balazs, W. Godbey, Liposomes for use in gene delivery, J Drug Deliv 2011 (2011) 326497.

[57] Y.Y. Tam, S. Chen, P.R. Cullis, Advances in Lipid Nanoparticles for siRNA Delivery, Pharmaceutics 5(3) (2013) 498-507.

[58] Y. Sato, H. Hatakeyama, Y. Sakurai, M. Hyodo, H. Akita, H. Harashima, A

pH-sensitive cationic lipid facilitates the delivery of liposomal siRNA and gene silencing activity in vitro and in vivo, J Control Release 163(3) (2012) 267-76.

[59] H. Wang, C.A. Thorling, X. Liang, K.R. Bridle, J.E. Grice, Y. Zhu, D.H.G. Crawford, Z.P. Xu, X. Liu, M.S. Roberts, Diagnostic imaging and therapeutic application of nanoparticles targeting the liver, Journal of Materials Chemistry B 3(6) (2015) 939-958.

[60] J. Wolfram, K. Suri, Y. Yang, J. Shen, C. Celia, M. Fresta, Y. Zhao, H. Shen, M. Ferrari, Shrinkage of pegylated and non-pegylated liposomes in serum, Colloids Surf B Biointerfaces 114 (2014) 294-300.

[61] M.N. Jones, A.R. Nicholas, The effect of blood serum on the size and stability of phospholipid liposomes, Biochim Biophys Acta 1065(2) (1991) 145-52.

[62] Z. Cao, N.N.M. Adnan, G. Wang, A. Rawal, B. Shi, R. Liu, K. Liang, L. Zhao, J.J. Gooding, C. Boyer, Z. Gu, Enhanced colloidal stability and protein resistance of layered double hydroxide nanoparticles with phosphonic acid-terminated PEG coating for drug delivery, J Colloid Interface Sci 521 (2018) 242-251.

[63] J.S. Suk, Q. Xu, N. Kim, J. Hanes, L.M. Ensign, PEGylation as a strategy for improving nanoparticle-based drug and gene delivery, Adv Drug Deliv Rev

99(Pt A) (2016) 28-51.

[64] Y. Bao, Y. Jin, P. Chivukula, J. Zhang, Y. Liu, J. Liu, J.P. Clamme, R.I. Mahato, D. Ng, W. Ying, Y. Wang, L. Yu, Effect of PEGylation on biodistribution and gene silencing of siRNA/lipid nanoparticle complexes, Pharm Res 30(2) (2013) 342-51.

[65] L.-Y. Zhou, Y.-H. Zhu, X.-Y. Wang, C. Shen, X.-W. Wei, T. Xu, Z.-Y. He, Novel zwitterionic vectors: Multi-functional delivery systems for therapeutic genes and drugs, Computational and Structural Biotechnology Journal 18 (2020) 1980-1999.

[66] M.J. Geisow, W.H. Evans, pH in the endosome. Measurements during pinocytosis and receptor-mediated endocytosis, Exp Cell Res 150(1) (1984) 36-46.

[67] R.K. Jain, T. Stylianopoulos, Delivering nanomedicine to solid tumors, Nat Rev Clin Oncol 7(11) (2010) 653-64.

[68] V. Zinchuk, O. Zinchuk, T. Okada, Quantitative colocalization analysis of multicolor confocal immunofluorescence microscopy images: pushing pixels to explore biological phenomena, Acta Histochem Cytochem 40(4) (2007) 101-11.

[69] M. Maugeri, M. Nawaz, A. Papadimitriou, A. Angerfors, A. Camponeschi, M. Na, M. Hölttä, P. Skantze, S. Johansson, M. Sundqvist, J. Lindquist, T.

Kjellman, I.-L. Mårtensson, T. Jin, P. Sunnerhagen, S. Östman, L. Lindfors, H. Valadi, Linkage between endosomal escape of LNP-mRNA and loading into EVs for transport to other cells, Nature Communications 10(1) (2019) 4333.

[70] J. Gilleron, W. Querbes, A. Zeigerer, A. Borodovsky, G. Marsico, U. Schubert, K. Manygoats, S. Seifert, C. Andree, M. Stöter, H. Epstein-Barash, L. Zhang, V. Koteliansky, K. Fitzgerald, E. Fava, M. Bickle, Y. Kalaidzidis, A. Akinc, M. Maier, M. Zerial, Image-based analysis of lipid nanoparticle-mediated siRNA delivery, intracellular trafficking and endosomal escape, Nat Biotechnol 31(7) (2013) 638-46.

[71] S.L.Y. Teo, J.J. Rennick, D. Yuen, H. Al-Wassiti, A.P.R. Johnston, C.W. Pouton, Unravelling cytosolic delivery of cell penetrating peptides with a quantitative endosomal escape assay, Nature Communications 12(1) (2021) 3721.

[72] S. Dutta, B.G. Watson, S. Mattoo, J.C. Rochet, Calcein Release Assay to Measure Membrane Permeabilization by Recombinant Alpha-Synuclein, Bio Protoc 10(14) (2020).

[73] H. Han, RNA Interference to Knock Down Gene Expression, Methods Mol Biol 1706 (2018) 293-302.

[74] A.K. Nair, L.J. Baier, Using Luciferase Reporter Assays to Identify

Functional Variants at Disease-Associated Loci, Methods Mol Biol 1706 (2018) 303-319.

[75] C. Remsburg, K. Konrad, N.F. Sampilo, J.L. Song, Analysis of microRNA functions, Methods Cell Biol 151 (2019) 323-334.

[76] T. Bus, A. Traeger, U.S. Schubert, The great escape: how cationic polyplexes overcome the endosomal barrier, Journal of Materials Chemistry B 6(43) (2018) 6904-6918.

[77] Y. Ding, Z. Jiang, K. Saha, C.S. Kim, S.T. Kim, R.F. Landis, V.M. Rotello, Gold nanoparticles for nucleic acid delivery, Mol Ther 22(6) (2014) 1075-1083.

[78] Y. Li, R. Liu, Y. Shi, Z. Zhang, X. Zhang, Zwitterionic poly(carboxybetaine)-based cationic liposomes for effective delivery of small interfering RNA therapeutics without accelerated blood clearance phenomenon, Theranostics 5(6) (2015) 583-96.

[79] Z. Cao, L. Zhang, S. Jiang, Superhydrophilic zwitterionic polymers stabilize liposomes, Langmuir 28(31) (2012) 11625-32.

[80] A. Erfani, J. Seaberg, C.P. Aichele, J.D. Ramsey, Interactions between Biomolecules and Zwitterionic Moieties: A Review, Biomacromolecules 21(7) (2020) 2557-2573.

[81] A.J. Keefe, S. Jiang, Poly(zwitterionic)protein conjugates offer increased

stability without sacrificing binding affinity or bioactivity, Nat Chem 4(1) (2011) 59-63.

[82] C.J. Smith, A.M. Osborn, Advantages and limitations of quantitative PCR (Q-PCR)-based approaches in microbial ecology, FEMS Microbiol Ecol 67(1) (2009) 6-20.

[83] C. Aranha, V. Patel, V. Bhor, D. Gogoi, Cycle threshold values in RT-PCR to determine dynamics of SARS-CoV-2 viral load: An approach to reduce the isolation period for COVID-19 patients, J Med Virol 93(12) (2021) 6794-6797.

[84] B. Spänkuch-Schmitt, J.r. Bereiter-Hahn, M. Kaufmann, K. Strebhardt, Effect of RNA Silencing of Polo-Like Kinase-1 (PLK1) on Apoptosis and Spindle Formation in Human Cancer Cells, JNCI: Journal of the National Cancer Institute 94(24) (2002) 1863-1877.

[85] K. Shiraishi, K. Kawano, Y. Maitani, T. Aoshi, K.J. Ishii, Y. Sanada, S. Mochizuki, K. Sakurai, M. Yokoyama, Exploring the relationship between anti-PEG IgM behaviors and PEGylated nanoparticles and its significance for accelerated blood clearance, Journal of controlled release : official journal of the Controlled Release Society 234 (2016) 59-67.

[86] B.G. Carvalho, B.T. Ceccato, M. Michelon, S.W. Han, L.G. de la Torre, Advanced Microfluidic Technologies for Lipid Nano-Microsystems from

Synthesis to Biological Application, Pharmaceutics 14(1) (2022).